

Delivery-Aware Cooperative Joint Multi-Bitrate Video Caching and Transcoding in 5G

Sepehr Rezvani, Saeedeh Parsaeefard, *Member, IEEE*, Nader Mokari, *Member, IEEE*, Mohammad R. Javan, *Member, IEEE*, and Halim Yanikomeroglu, *Fellow, IEEE*

Abstract

This paper proposes a two-phase resource allocation framework (RAF) for a parallel cooperative joint multi-bitrate video caching and transcoding (CVCT) in heterogeneous virtualized mobile-edge computing (HV-MEC) networks. In the cache placement phase, we propose delivery-aware cache placement strategies (DACPSs) based on the available video popularity distribution (VPD) and channel distribution information (CDI) to exploit the flexible delivery opportunities, i.e., video transmission and transcoding capabilities. Then, for the delivery phase, we propose a delivery policy for given caching status, instantaneous requests of users, and channel state information (CSI). The optimization problems corresponding to both phases aim to maximize the total revenue of slices subject to the quality of services contracted between slices and end-users and the system constraints based on their own assumptions. Both problems are non-convex and suffer from their high-computational complexities. For each phase, we show how these two problems can be solved efficiently. We also design a low-complexity RAF (LC-RAF) in which the complexity of the delivery algorithm is significantly reduced. Extensive numerical assessments demonstrate up to 30% performance improvement of our proposed DACPSs over traditional approaches.

Index Terms– Mobile-edge computing, multi-bitrate video caching and transcoding, adaptive bitrate streaming, cooperative caching, delivery-aware video caching, 5G.

Sepehr Rezvani and Nader Mokari are with the Department of Electrical and Computer Engineering, Tarbiat Modares University, Tehran, Iran.

Saeedeh Parsaeefard is with Communication Technologies & Department, ITRC, Tehran, Iran.

Mohammad R. Javan is with the Department of Electrical and Robotics Engineering, Shahrood University of Technology, Shahrood, Iran.

H. Yanikomeroglu is with the Department of Systems and Computer Engineering, Carleton University, Ottawa, ON K1S 5B6, Canada (E-mail: halim@sce.carleton.ca).

I. INTRODUCTION

A. Background & Motivations

Wireless edge caching has been developed as a candidate solution to satisfy the high data rate and/or low latency multimedia services in the fifth generation (5G) mobile communication system and offload the scarce and expensive backhaul links by proactively storing contents at the edge of the wireless networks [1], [2]. According to the Cisco's study, over 78% of the global mobile data traffic will be video by 2021 [3]. In this way, more and more researchers' attention has been attracted to video caching at network edge [2], [4]–[8].

Due to the various existing specifications of a video file, service providers often need to transcode a video file into multiple bitrates [4], [5], [8], [9]. In doing so, adaptive bit rate (ABR) streaming techniques have been developed to enhance the quality of delivered video in radio access networks (RANs), where each video file is adjusted according to the users' requests based on their display size and network channel condition [4], [5], [8].

Recently, mobile edge computing (MEC) networks have provided the caching and computation capabilities at MEC servers [6], [10]–[12]. In this architecture, prefetching video files and the transcoding operations can take place close to the end-users which cause enormous latency and backhaul traffic reductions. However, transcoding a large number of videos at each limited processing capacity MEC server simultaneously, poses another challenge for delay-sensitive services. Therefore, we need to determine which bitrate variant of a video file should be cached or transcoded to another lower bitrate variant. However, this solution may waste storage and processing resources due to storing and transcoding the same video files at multiple MEC servers. In this line, cooperative joint multi-bitrate video caching and transcoding (CVCT) technology is developed, where each MEC server is able to receive the requested video files from neighbor MEC servers via the fronthaul links [5]. In this architecture, each MEC server is deployed side-by-side with each base station (BS) using the generic computing platforms which provides the caching and computation capabilities in heterogeneous networks (HetNets) [5], [6]. To reduce the capital expenses (CapEx) and operation expenses (OpEx) of RANs, wireless network virtualization technology is developed, where the wireless network infrastructure is abstracted and sliced based on different services [13]–[15]. Therefore, integration of the aforementioned technologies enables the CVCT technology at MEC servers, and network infrastructure abstraction for different cost-efficient wireless servicing.

Recently, designing efficient cache placement strategies (CPSs) under the consideration of transmission strategies has become more attractive to utilize the physical-layer delivery opportunities in order to have an efficient delivery performance [7], [8], [16], [17]. The flexibility of video CPSs can also be improved by simultaneously optimizing the storage, transmission and transcoding resources in the algorithm design. In other words, in contrast to conventional baseline popular/bitrate video CPSs, we can improve the performance of the video CPSs by utilizing the delivery opportunities, i.e., designing a delivery-aware CPS (DACPS). However, some methodologies need to be devised to handle the variations of channel state information (CSI) and instantaneous requests of users.

B. Related Works

Indeed, although the idea of storing popular contents in cache-assisted devices in RANs is somewhat recent, many research works have addressed the content placement and delivery problems from different aspects resulting in an extensive literature. All research works in the context of content caching is classified into two categories: 1) delivery performance analysis for different CPSs; 2) designing CPSs in order to have an efficient delivery performance. In the first category, the benefits of designing efficient user association as well as radio resource allocation for different certain CPSs is investigated in [18] and [19]. In [18], the authors proposed a joint resource allocation and user association algorithm in orthogonal frequency division multiple access (OFDMA)-based fronthaul capacity constrained cloud-RANs (C-RANs) in order to minimize the networks delivery cost. The work in [19] devises a joint resource allocation and user association algorithm in HetNets with device-to-device (D2D) communications to maximize the user's revenue. In the second category, some existing works investigate the benefits of considering the transmission opportunities in the CPS design for different cache-assisted schemes, such as backhaul-limited networks [2], [7], [13], [20], cooperative transmission based networks [17], [21], cooperative caching networks [22], joint cooperative caching and transmission networks [1], [16], non-orthogonal multiple access (NOMA) based networks [23], and network virtualization [13]–[15], [24].

In the context of cloud-based video transcoding, some research efforts investigate the advantages of cloud computing and devise joint processing resource allocation and scheduling policies to reduce the transcoding delays in the delivery phase [9], [25]. In addition, the works in [4], [5], [8] investigate the joint multi-bitrate video caching and transcoding by utilizing the

ABR streaming technology in C-RANs. In [4], a transmission-aware joint multi-bitrate video caching and transcoding policy is devised to maximize the number and quality of concurrent video requests in each time slot in a single-cell scenario. In [8], the benefits of joint caching and radio resource allocation policy is investigated for a multi-cell MEC network without any cooperation between MEC servers. The authors in [5] investigate the design of a CVCT policy with user association and request scheduling to minimize the network delivery cost where they only focus on devising a cache replacement strategy in the online delivery phase based on the arrival video requests. Although they design a transcoding-aware cache replacement strategy, they did not consider the effect of the transmission opportunities, as well as the channel capacity of access and fronthaul links which should be carefully handled, specifically in cooperative fronthaul constrained mesh networks to satisfy the quality of service (QoS) at end-users.

C. Our Contributions

In this paper, we consider a network architecture with 10+ enabling technologies can imagine put together in 5G which is named as parallel CVCT system in a multicarrier NOMA (MC-NOMA)-assisted heterogeneous virtualized MEC (HV-MEC) network. This network consists of multiple remote radio systems (RRSs) each of which is equipped with a BS and a MEC server that enables the CVCT capability in the network. In this system, we propose a virtualization model and a pricing scheme based on the revenues of slices with a specific QoS. We aim at maximizing the revenue of slices by efficiently exploiting the limited physical resources as storage, processing, and transmission.

In this work, we first propose a resource allocation framework (RAF) in which the network operation time is divided into two phases called cache placement phase (Phase 1) and delivery phase (Phase 2). To the best of our knowledge, this paper is the first in the literature which investigates the idea of deploying efficient delivery-aware CPSs (DACPSs) in a parallel CVCT system for HV-MEC based on the available stochastic wireless channel distribution information (CDI) and video popularity distribution (VPD). This novel strategy is designed based on recent technologies in 5G by jointly allocating available physical resources and associating users to RRSs with request scheduling. This novel idea can also be used in closed to almost all cache-assisted wireless networks.

In simulation results, we answer the question of “*which of these technologies contribute most to the observed gain?*” by investigating the performance gain achieved by each technology alone

in the system. This work can be considered as a benchmark for future related works in HV-MECs. To the best of our knowledge, this paper is the first in the literature that investigates the effect of utilizing the MC-NOMA technology in the bandwidth cost reduction in the virtualization context. Besides, we show that our proposed DACPSs have between 25% and 40% improvement in the total delivery revenue of slices compared to the conventional baseline video popularity/bitrate strategies.

This paper also provides a solution to reduce the computational complexity of our delivery algorithm in Phase 2 with on-demand and real-time cloud services. In doing so, we propose a low-complexity RAF (LC-RAF) where some policies in Phase 1 are directly adopted for the next Phase 2. We show that our proposed LC-RAF can be efficiently utilized for dense environments with higher levels of the large-scale fading.

D. Paper Organization

The rest of this paper is organized as follows. Section II presents the considered network architecture and formulates the cache placement and delivery optimization problems. Section III provides the solution of the main problems. The proposed LC-RAF is also presented in this section. The numerical results are presented in Section IV. Our concluding remarks are provided in Section V.

II. SYSTEM MODEL AND PROBLEM FORMULATION

A. Network Architecture and System Settings

Consider a multiuser HV-MEC consisting of multiple RRSs where each of them is equipped with one type of access node, e.g., macro BS (MBS) or femto BS (FBS), and a MEC server that enables video caching and transcoding capabilities at the RRS [5], [6]. The set of users and RRSs are denoted by $\mathcal{U} = \{1, \dots, U\}$ and $\mathcal{B} = \{1, \dots, B\}$, respectively. All RRSs are connected together via limited wired fronthaul mesh network which provides the cooperative communication between RRSs. An origin cloud server denoted by 0 is connected to each RRS via a limited wired backhaul link. Here, we assume that a hypervisor enables the virtualization of the network where the physical infrastructure provider (InP) is abstracted into a set of $\mathcal{M} = \{1, \dots, M\}$ virtual networks, i.e., slices, such that slice m has owned a subset of users in \mathcal{U} , i.e., \mathcal{U}_m , and is responsible for providing a specific QoS for its own users [13], [15]. We assume that each user is subscribed to only one slice. Fig. 1 shows an illustration of this network.

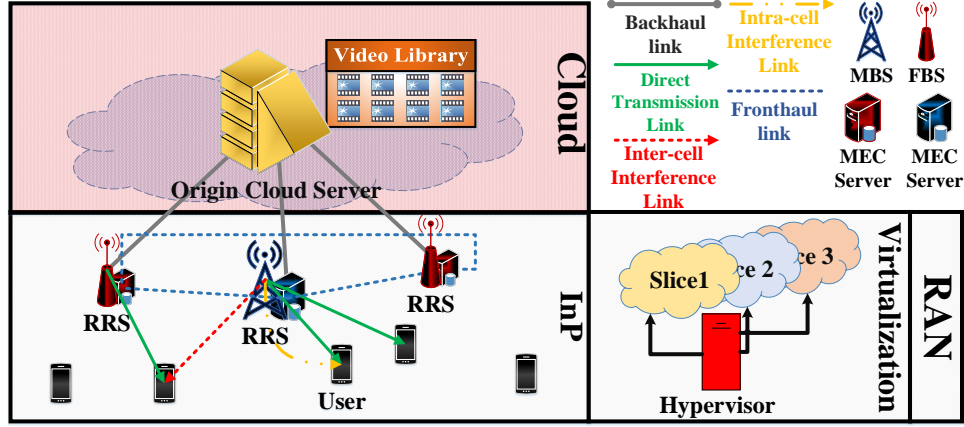


Fig. 1: An example of the multiuser HV-MEC architecture consisting of 3 RRSs, 3 slices, and one InP.

Assume that there exists V unique transcodable videos, each having L bitrate variants¹ in the origin cloud server with unlimited storage capacity [5], [8], [17]. The video library is denoted by $\mathcal{V} = \left\{ v_l | v \in \{1, \dots, V\}, l \in \{1, \dots, L\} \right\}$, where v_l belongs to the v^{th} video type with the l^{th} bitrate variant with the size of s_{v_l} . Consider that video v_h can be transcoded to v_l if $l < h$ [4]–[6]. Note that $s_{v_l} \leq s_{v_h}$ if $l \leq h$ [5].

The considered network operates in two phases as: Phase 1 in which the scheduled video files are proactively stored in the cache of RRSs during off-peak times [4], [5]; Phase 2 in which the requested videos are sent to the end-users based on the adopted delivery policy [5], [9], [25], [26]. In Phase 1, we aim to design an efficient DACPS based on the available VPD and CDI and cover the whole Phase 2. Phase 2 followed by Phase 1 is divided into multiple finite time slots, where in each time slot, we propose a delivery policy based on the available requests of users, CSI and the caching status. The proposed RAF is illustrated in Fig. 2. In the following, we first describe the delivery model in Phase 2 and then, we investigate the idea of developing DACPSs in Phase 1 based on the considered delivery model.

B. Delivery Phase

Assume that this phase is divided into multiple time slots where at each time slot, each user requests one video file [17], [27]. Also, the CSI and requests of users remain fixed through a

¹The lowest bitrate of each video type is denoted by 1 and the highest is denoted by L .

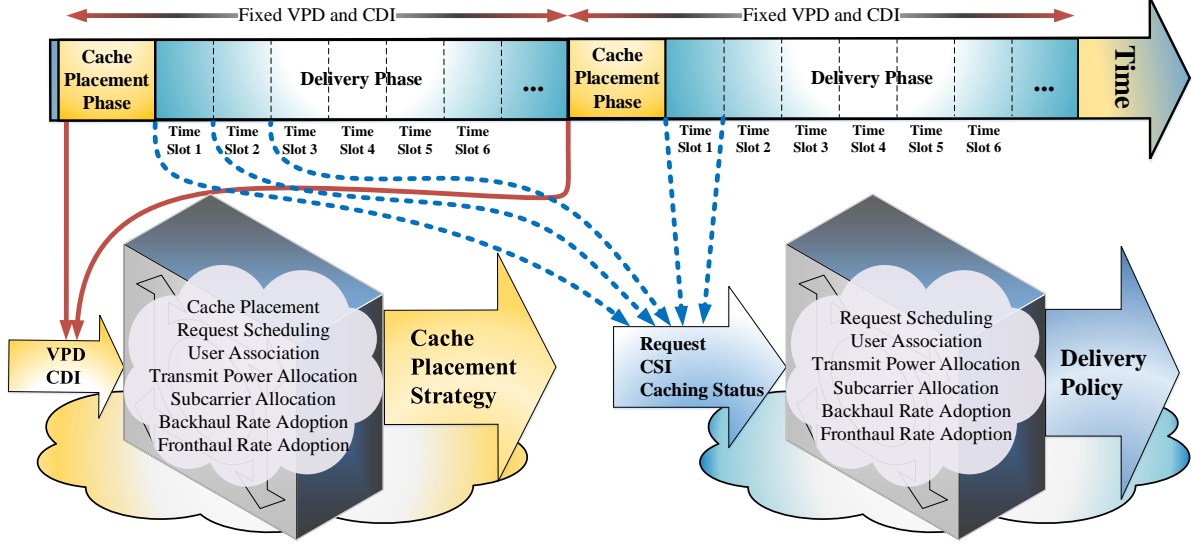


Fig. 2: The scheme of the proposed two-phase RAF for parallel CVCT system in HV-MECs.

time slot and are completely independent from other time slots², and all requests of users at each time slot are served within that time slot [13], [27]. Hence, the adopted delivery policy for each time slot is completely independent from other time slots. Therefore, we focus on only one time slot in Phase 2 where the request of user u for video v_l is indicated by a binary variable $\delta_u^{v_l} \in \{0, 1\}$ such that if user u requests video v_l , $\delta_u^{v_l} = 1$ and otherwise, $\delta_u^{v_l} = 0$. Thus, we have $\sum_{v_l \in \mathcal{V}} \delta_u^{v_l} = 1, \forall u \in \mathcal{U}$. The binary parameter $\theta_{b,u} \in \{0, 1\}$ determines the user association indicator, where if user u is associated to RRS b , $\theta_{b,u} = 1$ and otherwise, $\theta_{b,u} = 0$. In this system, we assume that each user can be connected to at most one RRS which is represented as

$$\sum_{b \in \mathcal{B}} \theta_{b,u} \leq 1, \quad \forall u \in \mathcal{U}. \quad (1)$$

The requests of users associated to RRS b for video v_l can be served by one of the following binary events denoted by

- 1) $x_b^{v_l} = 1$ represents that video v_l can be sent directly from cache of RRS b .
- 2) $y_b^{v_h, v_l} = 1$ indicates that video v_l is directly served by RRS b after being transcoded from a higher bitrate variant h at RRS b .

²In contrast to the closed to almost prior works in which the CSI is assumed to be fixed in all phases, in this paper, we aim to consider a near realistic scenario in which the CSI varies between different time slots of Phase 2 and is non-achievable during Phase 1.

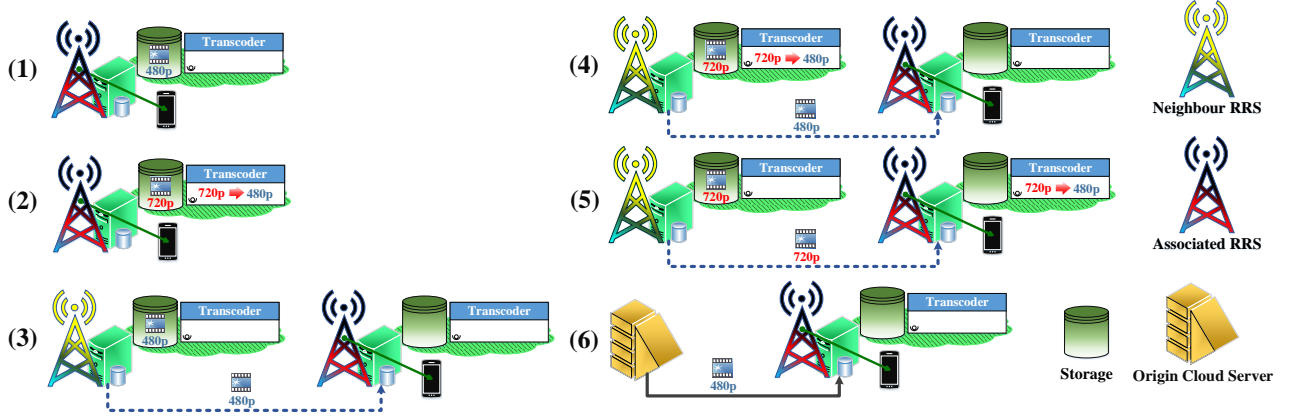


Fig. 3: The possible events of serving a request of a user in the CVCT system. We assume that there are two bitrate variants of a video file as 480p and 720p, where the user requests the 480p bitrate variant.

- 3) $z_{b',b}^{v_l} = 1$ denotes that video v_l is provided from cache of RRS $b' \neq b$ via fronthaul link.
- 4) $t_{b',b}^{v_h,v_l} = 1$ represents that video v_l is served by transcoding from $v_h, h > l$ at RRS $b' \neq b$ and then, sending to RRS b via fronthaul link.
- 5) $w_{b',b}^{v_h,v_l} = 1$ indicates that video v_l is obtained by sending video $v_h, h > l$ from RRS b' to RRS b via fronthaul link and then, transcoding v_h to v_l at RRS b .
- 6) $o_b^{v_l} = 1$ represents that the requests of users of RRS b for video v_l are served from the origin cloud server via backhaul link b .

Fig. 3 shows all possible events which happen to serve requests for each video file at each RRS. To avoid duplicated video provisioning at each RRS, we assume that all the requests for each video file v_l from users associated to RRS b can be served by only one type of events [5], i.e.,

$$x_b^{v_l} + \sum_{\substack{v_h \in \mathcal{V} \\ h > l}} y_b^{v_h,v_l} + \sum_{\substack{b' \in \mathcal{B} \\ b' \neq b}} z_{b',b}^{v_l} + \sum_{\substack{b' \in \mathcal{B} \\ b' \neq b}} \sum_{\substack{v_h \in \mathcal{V} \\ h > l}} (t_{b',b}^{v_h,v_l} + w_{b',b}^{v_h,v_l}) + o_b^{v_l} = \min\left\{\sum_{u=1}^U \delta_u^{v_l} \theta_{b,u}, 1\right\}, \forall b \in \mathcal{B}, v_l \in \mathcal{V}. \quad (2)$$

Practically, the video transcoding can only be performed for higher bitrate variants of a transcodable video file to lower bitrate variants. Accordingly, we have $y_b^{v_h,v_l}, t_{b',b}^{v_h,v_l}, w_{b',b}^{v_h,v_l} = 0, \forall h \leq l$ [5], [9]. Note that each event can be chosen if the required video exists in the target storage [4], [5], [9]. Let $\rho_b^{v_l}$ be the binary cache placement indicator, where $\rho_b^{v_l} = 1$ if video v_l is cached by RRS b , and $\rho_b^{v_l} = 0$, otherwise. Therefore, we have

$$x_b^{v_l} \leq \rho_b^{v_l}, \quad y_b^{v_h,v_l} \leq \rho_b^{v_h}, \quad z_{b',b}^{v_l} \leq \rho_{b'}^{v_l}, \quad t_{b',b}^{v_h,v_l} \leq \rho_{b'}^{v_h}, \quad w_{b',b}^{v_h,v_l} \leq \rho_{b'}^{v_h}. \quad (3)$$

The MC-NOMA technology is deployed at each RRS such that the total frequency bandwidth W is divided into a set of $\mathcal{N} = \{1, 2, \dots, N\}$ orthogonal subcarriers, where the frequency band

of each subcarrier is W_s . MC-NOMA allows each orthogonal subcarrier n to be shared among multiple users in each RRS via applying a superposition coding at the transmitter side and a successive interference cancellation (SIC) at the receiver side [28]–[30]. The binary subcarrier assignment indicator is also indicated by $\tau_{b,u}^n$, where if subcarrier n is assigned to the channel from RRS b to user $u \in \mathcal{U}$, $\tau_{b,u}^n = 1$ and otherwise, $\tau_{b,u}^n = 0$. Note that each user can take subcarriers from RRS b if the user is associated with that RRS. Therefore, we should have [13]

$$\tau_{b,u}^n \leq \theta_{b,u}, \forall b \in \mathcal{B}, n \in \mathcal{N}, u \in \mathcal{U}. \quad (4)$$

We denote by $p_{b,u}^n$ the transmit power of RRS b to user $u \in \mathcal{U}$ on subcarrier n , and, $h_{b,u}^n$ the instantaneous channel power gain between RRS b and user $u \in \mathcal{U}$ on subcarrier n . After performing SIC, the instantaneous SINR at user $u \in \mathcal{U}$ associated to RRS b on subcarrier n is [28], [30]

$$\gamma_{b,u}^n = \frac{p_{b,u}^n h_{b,u}^n}{I_{b,u}^{\text{Intra},n} + I_{b,u}^{\text{Inter},n} + \sigma_{b,u}^n}, \quad (5)$$

where $I_{b,u}^{\text{Intra},n} = \sum_{\substack{u' \in \mathcal{U}, u' \neq u \\ h_{b,u'}^n > h_{b,u}^n}} p_{b,u'}^n h_{b,u'}^n$ represents the induced intra-cell interference on user $u \in \mathcal{U}$ over subcarrier n , $I_{b,u}^{\text{Inter},n} = \sum_{\substack{b' \in \mathcal{B} \\ b' \neq b}} \sum_{\substack{u' \in \mathcal{U}_s \\ u' \neq u}} p_{b',u'}^n h_{b',u'}^n$ is the received inter-cell interference at user $u \in \mathcal{U}$ over subcarrier n , and $\sigma_{b,u}^n = W_s N_0$ is the additive white Gaussian noise (AWGN) power, in which N_0 is the noise power spectral density (PSD). Therefore, the instantaneous data rate at user $u \in \mathcal{U}$ from RRS b on subcarrier n is $r_{b,u}^n = \tau_{b,u}^n W_s \log_2(1 + \gamma_{b,u}^n)$. To develop the SIC cancellation of MC-NOMA, the following constraint should be satisfied [30]

$$\tau_{b,u}^n \frac{p_{b,u}^n h_{b,u}^n}{\sum_{\substack{v \in \mathcal{U}, v \neq u' \\ h_{b,v}^n > h_{b,u'}^n}} p_{b,v}^n h_{b,v}^n + I_{b,u}^{\text{Inter},n} + \sigma_{b,u}^n} > \tau_{b,u'}^n \gamma_{b,u'}^n, \forall b \in \mathcal{B}, u, u' \in \mathcal{U}, n \in \mathcal{N}, \tau_{b,u}^n, \tau_{b,u'}^n > 0, h_{b,u}^n > h_{b,u'}^n. \quad (6)$$

Accordingly, the instantaneous data rate at user $u \in \mathcal{U}$ assigned to RRS b is $r_{b,u}^{\text{Ac}} = \sum_{n=1}^N r_{b,u}^n$. Under the assumption that each RRS b has a maximum transmit power P_b^{\max} , we have

$$\sum_{u \in \mathcal{U}} \sum_{n=1}^N \tau_{b,u}^n p_{b,u}^n \leq P_b^{\max}, \forall b \in \mathcal{B}. \quad (7)$$

Consequently, the instantaneous latency of user u to receive video v_l from RRS b can be calculated as $D_{b,u}^{\text{Ac},v_l} = \frac{s_{v_l}}{r_{b,u}^{\text{Ac}}}$.

Transcoding video v_h to $v_l, \forall l < h$, is performed via the ABR streaming technique in which the transcoding operation is mapped to a η^{v_h, v_l} -bits computation-intensive task [5], [6]. Let $N_{\text{Cycle}}^{v_h, v_l}$ be the number of central processing unit (CPU) cycles required to compute 1 bit of the

computation-intensive task of transcoding video³ v_h to v_l [10], [11]. Each RRS performs all scheduled computation tasks in parallel by efficiently allocating its computation resources [12]. The number of CPU cycles per second allocated to RRS b for transcoding video v_h to v_l is also indicated by $\phi_b^{v_h, v_l} \in \{0, 1, 2, \dots\}$ [9], [11], [25]. Let χ_b^{\max} be the maximum processing capacity of RRS b . Therefore, the per-RRS maximum processing capacity constraint can be expressed as

$$\sum_{\substack{v_h \in \mathcal{V} \\ h > l}} \sum_{v_l \in \mathcal{V}} \left(y_b^{v_h, v_l} + \sum_{b' \in \mathcal{B}/\{b\}} t_{b, b'}^{v_h, v_l} + \sum_{b' \in \mathcal{B}/\{b\}} w_{b', b}^{v_h, v_l} \right) \phi_b^{v_h, v_l} \leq \chi_b^{\max}, \forall b \in \mathcal{B}. \quad (8)$$

The speed of the transcoding process is obtained by the video transrating, i.e., transcoding bit rate, which is the number of bits are transcoded by the processor per second [26]. Therefore, the delay of transcoding video v_h to v_l at RRS b can be obtained by $D_b^{\text{TC}, v_h, v_l} = \frac{\eta^{v_h, v_l} N_{\text{Cycle}}^{v_h, v_l}}{\phi_b^{v_h, v_l}}$ [10], [12].

For this setup, we consider $R_{0, b}^{\max}$ and $R_{b', b}^{\max}$ as the maximum capacity of backhaul link b , and fronthaul link from RRS b' to RRS b , respectively [31]. We also denote $r_{0, b}^{v_l}$ and $r_{b', b}^{v_l}$ the adopted data rate for RRS b to receive video v_l from the origin cloud server and neighbor RRS b' , respectively. Hence, the following maximum channel capacity constraints should be satisfied

$$\sum_{v_l \in \mathcal{V}} o_b^{v_l} r_{0, b}^{v_l} \leq R_{0, b}^{\max}, \forall b \in \mathcal{B}, \quad (9)$$

and

$$\sum_{v_l \in \mathcal{V}} \left(z_{b', b}^{v_l} + \sum_{\substack{v_h \in \mathcal{V} \\ h > l}} t_{b', b}^{v_h, v_l} \right) r_{b', b}^{v_l} + \sum_{v_l \in \mathcal{V}} \sum_{\substack{v_h \in \mathcal{V} \\ h > l}} w_{b', b}^{v_h, v_l} r_{b', b}^{v_h} \leq R_{b', b}^{\max}, \forall b, b' \in \mathcal{B}, b' \neq b. \quad (10)$$

Accordingly, the delays of receiving video v_l from origin cloud server and RRS b' at RRS b are represented as $D_{0, b}^{\text{BH}, v_l} = \frac{s_{v_l}}{r_{0, b}^{v_l}}$ and $D_{b', b}^{\text{FH}, v_l} = \frac{s_{v_l}}{r_{b', b}^{v_l}}$, respectively.

From the isolation perspective in slicing context, to guarantee the QoS at users owned by each slice m , i.e., \mathcal{U}_m , we apply a minimum data rate constraint as⁴

$$\sum_{b \in \mathcal{B}} r_{b, u}^{\text{Ac}} \geq R_m^{\min}, \forall m \in \mathcal{M}, u \in \mathcal{U}_m, \quad (11)$$

³ $N_{\text{Cycle}}^{v_h, v_l}$ is referred to the workload of the task of transcoding video v_h to v_l in the ABR technique.

⁴We assume that each user aims to download a video file and each slice has a determined QoS for its own users. Online video servicing based on the playback rate of videos in HV-MECs is considered as a future work.

where R_m^{\min} represents the minimum required access data rate of users in \mathcal{U}_m [24]. The video transcoding process runs in parallel with the video transmission where the delay of each transcoding in the system is measured by transcoding the first several segments of a video file [9], [26] and is negligible compared to the corresponding wireless transmission delay. To efficiently allocate the physical resources in this parallel system, some transmission/transcoding delay constraints should be held for each multi-hop scheduling event. For instance, in Event 2, the delay of transcoding video v_h to v_l at RRS b should not be greater than the access latency of user u to receive video v_l from RRS b [4], [26], i.e.,

$$y_b^{v_h, v_l} D_b^{\text{TC}, v_h, v_l} \leq \delta_u^{v_l} D_{b, u}^{\text{Ac}, v_l}. \quad (12)$$

For Event 3, the delay of fronthaul transmission should not be greater than the access delay [24], [27], [31]. Therefore, we have

$$z_{b', b}^{v_l} D_{b', b}^{\text{FH}, v_l} \leq \delta_u^{v_l} D_{b, u}^{\text{Ac}, v_l}. \quad (13)$$

For Event 4, the delay of transcoding and fronthaul transmission should not be greater than the fronthaul and access delays, respectively. These practical constraints can be represented as

$$t_{b', b}^{v_h, v_l} D_{b'}^{\text{TC}, v_h, v_l} \leq t_{b', b}^{v_h, v_l} D_{b', b}^{\text{FH}, v_l}, \quad (14)$$

$$t_{b', b}^{v_h, v_l} D_{b', b}^{\text{FH}, v_l} \leq \delta_u^{v_l} D_{b, u}^{\text{Ac}, v_l}. \quad (15)$$

For Event 5, each fronthaul and transcoding delay should not be greater than that of the transcoding and access delays, respectively. Hence, we have

$$w_{b', b}^{v_h, v_l} D_{b', b}^{\text{FH}, v_h} \leq w_{b', b}^{v_h, v_l} D_b^{\text{TC}, v_h, v_l}, \quad (16)$$

$$w_{b', b}^{v_h, v_l} D_b^{\text{TC}, v_h, v_l} \leq \delta_u^{v_l} D_{b, u}^{\text{Ac}, v_l}. \quad (17)$$

Finally, for Event 6, the backhaul delay should be equal or less than that of the access delay for each video transmission. Accordingly, we have

$$o_b^{v_l} D_{0, b}^{\text{BH}, v_l} \leq \delta_u^{v_l} D_{b, u}^{\text{Ac}, v_l}. \quad (18)$$

If all conditions in (12)-(18) hold, the total latency of each user comes from its access delay (wireless transmission delay) [17], [24], [26]. This parallel system prevents the extra fronthaul/backhaul transmission and video transcoding delays in the network.

Since slices lease the physical resources of InP, we intend to propose a new pricing model to represent this structure. For the access transmission resources, the unit price of transmit power and spectrum of RRS b are indicated by α_b^{Pow} per Watt and α_b^{Sub} per Hz, respectively [14], [24]. Moreover, the unit price of backhaul and fronthaul rates are defined as α^{BH} and α^{FH} per bps [24]. For the storage resources, each slice pays μ_b^{Cache} per bit to utilize the memory of RRS b [14]. The price of the processing resources usage at RRS b is also defined as μ_b^{Proc} per CPU cycle. On the other hand, each slice m gets rewards from its own users due to providing their access data rates [13], [14], [24]. We define ψ_m as the reward of slice m from each user $u \in \mathcal{U}_m$ per unit of received data rate (bit/s). Let consider that ψ_m is an increasing function of R_m^{\min} , i.e., for $m \neq m' \in \mathcal{M}$, when $R_m^{\min} \geq R_{m'}^{\min}$, $\psi_m \geq \psi_{m'}$. In this scheme, we aim to maximize the slices revenues which can be defined as the reward minus cost of each slice. The reward of each slice m is $\sum_{b \in \mathcal{B}} r_{b,u}^{\text{Ac}} \psi_m$. To define the cost of each slice, we first formulate the cost of provisioning video v_l to RRS b caused by one of the scheduling events, as

$$\begin{aligned} \mathbb{S}_b^{\text{Cost,RRS},v_l} = & x_b^{v_l} (s_{v_l} \mu_b^{\text{Cache}}) + \sum_{\substack{v_h \in \mathcal{V} \\ h > l}} y_b^{v_h, v_l} (s_{v_h} \mu_b^{\text{Cache}} + \phi_b^{v_h, v_l} \mu_b^{\text{Proc}}) + \sum_{\substack{b' \in \mathcal{B} \\ b' \neq b}} z_{b', b}^{v_l} (s_{v_l} \mu_{b'}^{\text{Cache}} + r_{b', b}^{v_l} \alpha^{\text{FH}}) + \\ & \sum_{\substack{b' \in \mathcal{B} \\ b' \neq b}} \sum_{\substack{v_h \in \mathcal{V} \\ h > l}} t_{b', b}^{v_h, v_l} (s_{v_h} \mu_{b'}^{\text{Cache}} + \phi_{b'}^{v_h, v_l} \mu_{b'}^{\text{Proc}} + r_{b', b}^{v_l} \alpha^{\text{FH}}) + \sum_{\substack{b' \in \mathcal{B} \\ b' \neq b}} \sum_{\substack{v_h \in \mathcal{V} \\ h > l}} w_{b', b}^{v_h, v_l} (s_{v_h} \mu_{b'}^{\text{Cache}} + r_{b', b}^{v_h} \alpha^{\text{FH}} + \\ & \phi_b^{v_h, v_l} \mu_b^{\text{Proc}}) + o_b^{v_l} (r_{0, b}^{v_l} \alpha^{\text{BH}}). \quad (19) \end{aligned}$$

Furthermore, the cost of access transmission resource usage for transferring the requested video file to user u is $\mathbb{S}_u^{\text{Cost,Ac}} = \sum_{b \in \mathcal{B}} \sum_{n \in \mathcal{N}} (p_{b,u}^n \alpha_b^{\text{Pow}} + \tau_{b,u}^n W_s \alpha_b^{\text{Sub}})$. Therefore, the cost of serving the request of user u for video v_l is $\mathbb{S}_u^{\text{Cost,User},v_l} = \delta_u^{v_l} \left(\mathbb{S}_u^{\text{Cost,Ac}} + \sum_{b \in \mathcal{B}} \theta_{b,u} \mathbb{S}_b^{\text{Cost,RRS},v_l} \right)$ which should be paid by slice m , if $u \in \mathcal{U}_m$. Hence, the revenue of each slice for serving video v_l to user $u \in \mathcal{U}_m$ is $\left(\sum_{b \in \mathcal{B}} r_{b,u}^{\text{Ac}} \psi_m - \mathbb{S}_u^{\text{Cost,User},v_l} \right)$.

Based on (2), each slice pays the cost of storage, processing, backhaul, and fronthaul resource usages for each video provisioning to each cell only once. Besides, each slice m pays the cost usage of each subcarrier only once in each cell, even the subcarrier be shared among users in \mathcal{U}_m in that cell via the MC-NOMA technology. Accordingly, the revenue of slice m in Phase 2 can be defined as

$$\mathbb{S}_m^{\text{slice}} = \sum_{u \in \mathcal{U}_m} \sum_{b \in \mathcal{B}} r_{b,u}^{\text{Ac}} \psi_m - \sum_{u \in \mathcal{U}_m} \sum_{b \in \mathcal{B}} \sum_{n \in \mathcal{N}} (p_{b,u}^n \alpha_b^{\text{Pow}}) - \sum_{b \in \mathcal{B}} \sum_{n \in \mathcal{N}} \left(\max_{u \in \mathcal{U}_m} \{ \tau_{b,u}^n \} W_s \alpha_b^{\text{Sub}} \right)$$

$$- \sum_{b \in \mathcal{B}} \sum_{v_l \in \mathcal{V}} \min \left\{ \sum_{u \in \mathcal{U}_m} \theta_{b,u} \delta_u^{v_l}, 1 \right\} \mathbb{S}_b^{\text{Cost,RRS},v_l}. \quad (20)$$

In Phase 2, with the objective of maximizing the total delivery revenue of slices denoted by $\mathbb{S}_{\text{tot}} = \sum_{m \in \mathcal{M}} \mathbb{S}_m^{\text{slice}}$ under the QoS requirements of users, we jointly optimize the user association, access transmit power and subcarrier allocation, fronthaul and backhaul rate adaption, processing resource allocation and request scheduling to have an efficient delivery performance. To ease of notations, we denote $\boldsymbol{\theta} = [\theta_{b,u}]$, $\boldsymbol{\phi} = [\phi_b^{v_h,v_l}]$, $\boldsymbol{p} = [p_{b,u}^n]$, $\boldsymbol{\tau} = [\tau_{b,u}^n]$, $\boldsymbol{r}^{\text{BH}} = [r_{0,b}^{v_l}]$, $\boldsymbol{r}^{\text{FH}} = [r_{b',b}^{v_l}]$, $\boldsymbol{\Upsilon} = [\boldsymbol{x}, \boldsymbol{y}, \boldsymbol{z}, \boldsymbol{t}, \boldsymbol{w}, \boldsymbol{o}]$, $\boldsymbol{x} = [x_b^{v_l}]$, $\boldsymbol{y} = [y_b^{v_h,v_l}]$, $\boldsymbol{z} = [z_{b',b}^{v_l}]$, $\boldsymbol{t} = [t_{b',b}^{v_h,v_l}]$, $\boldsymbol{w} = [w_{b',b}^{v_h,v_l}]$, and $\boldsymbol{o} = [o_b^{v_l}]$. The delivery optimization problem can be formulated as

$$\max_{\boldsymbol{\theta}, \boldsymbol{\phi}, \boldsymbol{p}, \boldsymbol{\tau}, \boldsymbol{r}^{\text{BH}}, \boldsymbol{r}^{\text{FH}}, \boldsymbol{\Upsilon}} \mathbb{S}_{\text{tot}} \quad (21a)$$

s.t. (1)-(4), (6), (7)-(18)

$$y_b^{v_h,v_l} = 0, t_{b',b}^{v_h,v_l} = 0, w_{b',b}^{v_h,v_l} = 0, \forall h \leq l, \quad (21b)$$

$$\sum_{u \in \mathcal{U}} \tau_{b,u}^n \leq \Psi_b, \forall b \in \mathcal{B}, n \in \mathcal{N}, \quad (21c)$$

$$\theta_{b,u}, \tau_{b,u}^n, x_b^{v_l}, y_b^{v_h,v_l}, z_{b',b}^{v_l}, t_{b',b}^{v_h,v_l}, w_{b',b}^{v_h,v_l}, o_b^{v_l} \in \{0, 1\}, \phi_b^{v_h,v_l} \in \{0, 1, 2, \dots\}, p_{b,u}^n, r_{0,b}^{v_l}, r_{b',b}^{v_l} \geq 0, \quad (21d)$$

where (21c) represents that in each cell b , each subcarrier n can be assigned to at most Ψ_b users [30].

C. Cache Placement Phase

In Phase 1, we consider that the requests and CSI of users are not available at the scheduler. To cover the whole Phase 1 in the CPS, we first assume that the VPD and the CDI are available at the scheduler in Phase 1 and do not change during the next Phase 2, i.e., are valid for the next Phase 2. In doing so, we assume that the CDI is averaged over various CSIs in different time slots. The VPD also follows the Zipf distribution with the Zipf parameter λ [17], [22] and is the same among all users in the network. Therefore, the popularity of requesting video v_l with rank⁵ Λ_{v_l} is given by $\Delta_{v_l} = \frac{1/(\Lambda_{v_l})^\lambda}{\sum_{v_l \in \mathcal{V}} 1/(\Lambda_{v_l})^\lambda}, \forall v_l \in \mathcal{V}$. To design a DACPS which covers the whole Phase 2, we propose an averaged based joint cache placement and ergodic resource allocation based on the VPD and CDI. Our DACPS is valid until the VPD and/or the CDI changes. In

⁵Consider that the videos in \mathcal{V} are randomly sorted from 1 to VL .

this scheme, the average or ergodic data rate of wireless access link between user u and RRS b is $\bar{r}_{b,u}^{\text{Ac}} = \mathbb{E}_{\mathbf{h}}\{r_{b,u}^{\text{Ac}}\}$, where $\mathbb{E}_{\mathbf{h}}\{\cdot\}$ is the expectation operator on the channel power gains. This expectation is necessary even in slow fading scenarios, since the whole Phase 2 has a much time length compared to the time duration of Phase 1. In this phase, in contrast to the instantaneous access delays formulated in Subsection II-B, the average access delay for receiving video v_l from RRS b at user u obtained by $\bar{D}_{b,u}^{\text{Ac},v_l} = \frac{s_{v_l}}{\bar{r}_{b,u}^{\text{Ac}}}$ is considered. Moreover, in order to apply SIC, the average SIC constraint should be satisfied as ⁶

$$\mathbb{E}_{\mathbf{h}}\left\{\tau_{b,u}^n \frac{p_{b,u'}^n h_{b,u}^n}{\sum_{\substack{v \in \mathcal{U}, v \neq u' \\ h_{b,v}^n > h_{b,u'}^n}} p_{b,v}^n h_{b,u}^n + I_{b,u}^{\text{Inter},n} + \sigma_{b,u}^n}\right\} > \mathbb{E}_{\mathbf{h}}\{\tau_{b,u'}^n \gamma_{b,u'}^n\}, \forall b \in \mathcal{B}, u, u' \in \mathcal{U}, n \in \mathcal{N},$$

$$\tau_{b,u}^n, \tau_{b,u'}^n > 0, \mathbb{E}_{\mathbf{h}}\{h_{b,u}^n\} > \mathbb{E}_{\mathbf{h}}\{h_{b,u'}^n\}. \quad (22)$$

Furthermore, constraint (2) in Phase 2 should be reformulated based on the VPD, since the requests of users are unknown in Phase 1. Formulating binary constraint (2) based on the VPD cannot be applied since all videos are requested based on their popularity. To tackle this challenge and cover all possible situations in Phase 2, we assume that all videos should be served by each RRS based on one of the events described in Fig. 3 if at least one user is associated to that RRS. Hence, we have

$$x_b^{v_l} + \sum_{\substack{v_h \in \mathcal{V} \\ h > l}} y_b^{v_h, v_l} + \sum_{\substack{b' \in \mathcal{B} \\ b' \neq b}} z_{b',b}^{v_l} + \sum_{\substack{b' \in \mathcal{B} \\ b' \neq b}} \sum_{\substack{v_h \in \mathcal{V} \\ h > l}} (t_{b',b}^{v_h, v_l} + w_{b',b}^{v_h, v_l}) + o_b^{v_l} = \min\left\{\sum_{u=1}^U \theta_{b,u}, 1\right\}, \forall b \in \mathcal{B}, v_l \in \mathcal{V}. \quad (23)$$

Although this constraint consumes more physical resources, it covers all possible situations. In other words, it guarantees that various sets of arrival requests in different time slots of Phase 2 can be served [5]. With this assumption and available CDI, constraints (12), (13), (15), (17), and (18) in Phase 2 are reformulated as

$$y_b^{v_h, v_l} D_b^{\text{TC}, v_h, v_l} \leq \bar{D}_{b,u}^{\text{Ac}, v_l}, \quad z_{b',b}^{v_l} D_{b',b}^{\text{FH}, v_l} \leq \bar{D}_{b,u}^{\text{Ac}, v_l}, \quad t_{b',b}^{v_h, v_l} D_{b',b}^{\text{FH}, v_l} \leq \bar{D}_{b,u}^{\text{Ac}, v_l},$$

$$w_{b',b}^{v_h, v_l} D_b^{\text{TC}, v_h, v_l} \leq \bar{D}_{b,u}^{\text{Ac}, v_l}, \quad o_b^{v_l} D_{0,b}^{\text{BH}, v_l} \leq \bar{D}_{b,u}^{\text{Ac}, v_l}, \quad (24)$$

⁶In contrast to Phase 2 in which the SIC cancellation is applied based on the CSI, in Phase 1, we apply SIC based on available CDI.

respectively. Let C_b^{\max} be the maximum storage capacity of RRS b . In contrast to Phase 2, in this phase, we add a cache size constraint for each RRS as follows:

$$\sum_{v_l \in \mathcal{V}} \rho_b^{v_l} s_{v_l} \leq C_b^{\max}, \forall b \in \mathcal{B}. \quad (25)$$

In Phase 1, our pricing model presented in Subsection II-B is also averaged based on both VPD and CDI. In this line, the average provisioning cost of a video file at RRS b can be formulated as $\bar{\Phi}_b^{\text{Cost,RRS}} = \sum_{v_l \in \mathcal{V}} \Delta_{v_l} \Phi_b^{\text{Cost,RRS},v_l}$. Moreover, the average reward of each slice m for providing a video file to user $u \in \mathcal{U}_m$ based on the considered average data rate $\bar{r}_{b,u}^{\text{Ac}}$ can be obtained by $\sum_{b \in \mathcal{B}} \bar{r}_{b,u}^{\text{Ac}} \psi_m$. Therefore, the average revenue of slice m is

$$\begin{aligned} \bar{\$}_m^{\text{slice}} = & \sum_{u \in \mathcal{U}_m} \sum_{b \in \mathcal{B}} \bar{r}_{b,u}^{\text{Ac}} \psi_m - \sum_{u \in \mathcal{U}_m} \sum_{b \in \mathcal{B}} \sum_{n \in \mathcal{N}} (p_{b,u}^n \alpha_b^{\text{Pow}}) - \sum_{b \in \mathcal{B}} \sum_{n \in \mathcal{N}} \left(\max_{u \in \mathcal{U}_m} \{\tau_{b,u}^n\} W_s \alpha_b^{\text{Sub}} \right) - \\ & \sum_{b \in \mathcal{B}} f_{b,m}(\boldsymbol{\theta}) \bar{\Phi}_b^{\text{Cost,RRS}}, \quad (26) \end{aligned}$$

where $f_{b,m}(\boldsymbol{\theta})$ is a function of $\theta_{b,u}$ which represents the number of specific videos in \mathcal{V} requested by users in \mathcal{U}_m associated to RRS b . The main challenge of (26) is obtaining an exact closed-form representation for $f_{b,m}(\boldsymbol{\theta})$ based on the available VPD which cannot be obtained, since the available VPD is independent from the user association process. Obviously, the value of $f_{b,m}(\boldsymbol{\theta})$ is upper-bounded by $\sum_{u \in \mathcal{U}_m} \theta_{b,u}$ and also is lower-bounded by $\min \left\{ \sum_{u \in \mathcal{U}_m} \theta_{b,u}, 1 \right\}$. Generally, the diversity of requesting video files affects $f_{b,m}(\boldsymbol{\theta})$. Specifically, if users have more diverse requests, i.e., $\lambda \rightarrow 0$, $f_{b,m}(\boldsymbol{\theta})$ increases which degrades the revenue of slices. Besides, if users have less diverse requests, i.e., $\lambda \rightarrow \infty$ or only a few video files are requested among all users, $f_{b,m}(\boldsymbol{\theta})$ decreases. Therefore, to obtain a closed-form representation for $f_{b,m}(\boldsymbol{\theta})$ in (26), we propose two low-diversity (LD) and high-diversity (HD) schemes. In the LD scheme, each slice assumes that all own users have the same request based on the VPD. Hence, this scheme considers the best requesting situation which provides the maximum achievable revenue of slices. Conversely, in the HD scheme, each slice assumes that all of its users have different requests, i.e., the worst requesting situation is considered. To handle the different requesting diversity situations in the CPS design, we propose two baseline diversity CPSs, namely LD and HD. In the LD strategy, we consider the upper-bound value of the average revenue of each slice formulated as

$$\bar{\$}_m^{\text{slice,UB}} = \sum_{u \in \mathcal{U}_m} \sum_{b \in \mathcal{B}} \bar{r}_{b,u}^{\text{Ac}} \psi_m - \sum_{u \in \mathcal{U}_m} \sum_{b \in \mathcal{B}} \sum_{n \in \mathcal{N}} (p_{b,u}^n \alpha_b^{\text{Pow}}) - \sum_{b \in \mathcal{B}} \sum_{n \in \mathcal{N}} \left(\max_{u \in \mathcal{U}_m} \{\tau_{b,u}^n\} W_s \alpha_b^{\text{Sub}} \right)$$

$$- \sum_{b \in \mathcal{B}} \min \left\{ \sum_{u \in \mathcal{U}_m} \theta_{b,u}, 1 \right\} \bar{\$}_b^{\text{Cost,RRS}}, \quad (27)$$

which is compatible with the LD scheme. On the other hand, for the HD strategy, we consider the lower-bound average revenue of each slice which is expressed as

$$\begin{aligned} \bar{\$}_m^{\text{slice,LB}} = & \sum_{u \in \mathcal{U}_m} \sum_{b \in \mathcal{B}} \bar{r}_{b,u}^{\text{Ac}} \psi_m - \sum_{u \in \mathcal{U}_m} \sum_{b \in \mathcal{B}} \sum_{n \in \mathcal{N}} (p_{b,u}^n \alpha_b^{\text{Pow}}) - \sum_{b \in \mathcal{B}} \sum_{n \in \mathcal{N}} \left(\max_{u \in \mathcal{U}_m} \{\tau_{b,u}^n\} W_s \alpha_b^{\text{Sub}} \right) \\ & - \sum_{b \in \mathcal{B}} \sum_{u \in \mathcal{U}_m} \theta_{b,u} \bar{\$}_b^{\text{Cost,RRS}}. \end{aligned} \quad (28)$$

This strategy is also compatible with the HD scheme. In this phase, we design DACPSs in the LD and HD schemes to maximize the total estimated average revenue of slices which are formulated as $\bar{\$}_{\text{tot}}^{\text{LD}} = \sum_{m \in \mathcal{M}} \bar{\$}_m^{\text{slice,UB}}$ and $\bar{\$}_{\text{tot}}^{\text{HD}} = \sum_{m \in \mathcal{M}} \bar{\$}_m^{\text{slice,LB}}$, respectively. The cache placement optimization problem in the LD scheme is

$$\max_{\rho, \theta, \phi, p, \tau, r^{\text{BH}}, r^{\text{FH}}, \Upsilon} \bar{\$}_{\text{tot}}^{\text{LD}} \quad (29a)$$

$$\text{s.t. } (1), (3), (4), (7)-(10), (14), (16), (21b)-(21d), (22)-(24),$$

$$\sum_{b \in \mathcal{B}} \bar{r}_{b,u}^{\text{Ac}} \geq R_m^{\min}, \forall m \in \mathcal{M}, u \in \mathcal{U}_m, \quad (29b)$$

$$\rho_b^{v_l} \in \{0, 1\}. \quad (29c)$$

The cache placement optimization problem in the HD scheme is

$$\max_{\rho, \theta, \phi, p, \tau, r^{\text{BH}}, r^{\text{FH}}, \Upsilon} \bar{\$}_{\text{tot}}^{\text{HD}} \quad (30a)$$

$$\text{s.t. } (1), (3), (4), (7)-(10), (14), (16), (21b)-(21d), (22)-(24), (29b), (29c).$$

Table I summarizes the main notations used in each phase.

The mixed-integer nonlinear programming (MINLP) problems (21), (29) and (30) are completely NP-hard which is mathematically proved in [32] in the transmit power and subcarrier allocation problem for MC-NOMA in order to maximize the downlink data rate of users. In addition, in [33], it is mentioned that data rate maximization optimization problems with interferences are completely NP-hard for OFDMA-based wireless networks and it is non-achievable to find the global optimum joint transmit power and subcarrier allocation policy by any existing method. Since the transmit power and subcarrier allocation in OFDMA is a special case of MC-NOMA [32], the result follows. The exhaustive search requires the examination of all $(2S^{\text{Power}})^{BUN} \cdot (2S^{\text{FH}})^{B^2VL} \cdot (8S^{\text{BH}})^{BVL} \cdot (2S^{\text{Process}})^{BVL^2} \cdot 2^{BU}$.

TABLE I: Main notations

Description	Notation	Phase	Description	Notation	Phase
Number of users	U	(1,2)	Number of RRSs	B	(1,2)
Number of slices	M	(1,2)	Number of unique videos	V	(1,2)
Number of bitrate variants	L	(1,2)	The v^{th} video type with the l^{th} bitrate variant	v_l	(1,2)
Size of video v_l	s_{v_l}	(1,2)	Request of user u for video v_l	$\delta_u^{v_l}$	2
User association indicator	$\theta_{b,u}$	(1,2)	Scheduling events	$(x_b^{v_l}, y_b^{v_l, v_l}, z_{b',b}^{v_l}, t_{b',b}^{v_l, v_l}, w_{b',b}^{v_l, v_l}, o_b^{v_l})$	(1,2)
Cache placement indicator	$\rho_b^{v_l}$	(1,2)	Number of subcarriers	N	(1,2)
Subcarrier assignment indicator	$\tau_{b,u}^n$	(1,2)	Transmit power	$p_{b,u}^n$	(1,2)
Instantaneous channel power gain	$h_{b,u}^n$	2	Instantaneous SINR	$\gamma_{b,u}^n$	2
Subcarrier bandwidth	W_s	(1,2)	Instantaneous data rate	$r_{b,u}^n$	2
AWGN noise power	$\sigma_{b,u}^n$	(1,2)	Instantaneous data rate	$r_{b,u}^n$	2
Maximum transmit power of each RRS	P_b^{\max}	(1,2)	Instantaneous access latency	$D_{b,u}^{\text{Ac}, v_l}$	2
Size of transcoding task	η^{v_h, v_l}	(1,2)	Workload of each transcoding task	$N_{\text{Cycle}}^{v_h, v_l}$	(1,2)
rocessing resource of each task	$\phi_b^{v_h, v_l}$	(1,2)	Maximum processing capacity of each RRS	χ_b^{\max}	(1,2)
Transcoding delay	$D_b^{\text{TC}, v_h, v_l}$	(1,2)	Backhaul capacity for each video	$r_{0,b}^{v_l}$	(1,2)
Fronthaul capacity for each video	$r_{b',b}^{v_l}$	(1,2)	Maximum capacity of each backhaul link	$R_{0,b}^{\max}$	(1,2)
Maximum capacity of each fronthaul link	$R_{b',b}^{\max}$	(1,2)	Backhaul delay	$D_{0,b}^{\text{BH}, v_l}$	(1,2)
Fronthaul delay	D_b^{FH, v_l}	(1,2)	Contracted minimum data rate at each slice	F_m^{\min}	(1,2)
Unit price of transmit power	α_b^{Pow}	(1,2)	Unit price of subcarrier	α_b^{Sub}	(1,2)
Unit price of backhaul capacity	α^{BH}	(1,2)	Unit price of fronthaul capacity	α^{FH}	(1,2)
Unit price of storage	μ_b^{Cache}	(1,2)	Unit price of processing	μ_b^{Proc}	(1,2)
Unit reward of each slice	ψ_m	(1,2)	Provisioning cost of each video at each slice	$\mathbb{S}_b^{\text{Cost}, \text{RRS}, v_l}$	2
Revenue of each slice	$\mathbb{S}_m^{\text{slice}}$	2	Total revenue of slices	\mathbb{S}_{tot}	2
Total revenue of slices	\mathbb{S}_{tot}	2	Maximum number of each user for each subcarrier	Ψ_b	(1,2)
Popularity of requesting videos	Δ_{v_l}	1	Average rate of each user	$\bar{r}_{b,u}^{\text{Ac}}$	1
Average latency at each user	$D_{b,u}^{\text{Ac}, v_l}$	1	Maximum storage capacity of each RRS	C_b^{\max}	1
Average provisioning cost of a video file at each RRS	$\mathbb{S}_b^{\text{Cost}, \text{RRS}}$	1	Average revenue of each slice	$\mathbb{S}_m^{\text{slice}}$	1
Number of videos requested by users in \mathcal{U}_m associated to RRS b	$f_{b,m}(\theta)$	1	Upper-bound of total average revenue of slices	$\mathbb{S}_{\text{tot}}^{\text{LD}}$	1
Lower-bound of total average revenue of slices	$\mathbb{S}_{\text{tot}}^{\text{HD}}$	1	-	-	-

$4^{B^2VL^2}$ possible situations, where S^{Power} , S^{FH} , S^{BH} and S^{Process} are the number of values that each variable in \mathbf{p} , \mathbf{r}^{FH} , \mathbf{r}^{BH} , and ϕ can take, respectively. Accordingly, it is very challenging and impractical to find the global optimum solution for such large-scale and NP-hard optimization problems, since the number of optimization variables and constraints grow exponentially [17], [19]–[21], [32].

The main structures of optimization problems (21) and (29) are the same for a fixed placement variable ρ . Therefore, we provide a local optimum resource allocation algorithm which can be adopted for both problems (21) and (29). However, (30) and (29) differ in objective function. Accordingly, we modify the solution algorithm proposed for (29) to be applied to (30).

III. DELIVERY-AWARE COOPERATIVE MULTI-BITRATE VIDEO CACHING AND TRANSCODING ALGORITHMS

This section provides solution algorithms for main problems (21), (29) and (30).

Algorithm 1 The main alternative method

- 1: Initialize $\Upsilon_0, \rho_0, \mathbf{p}_0, \phi_0, \mathbf{r}_0^{\text{FH}}, \mathbf{r}_0^{\text{BH}}, \tau_0$, and θ_0 .
 - repeat**
 - 2: **for** $\kappa_1 = 1$ to Γ_1 **do**
 - 3: **Step 1:** Find $(\mathbf{p}_{\kappa_1}, \phi_{\kappa_1}, \mathbf{r}_{\kappa_1}^{\text{FH}}, \mathbf{r}_{\kappa_1}^{\text{BH}})$ by solving (29) for a fixed $(\Upsilon_{\kappa_1-1}, \rho_{\kappa_1-1}, \tau_{\kappa_1-1}, \theta_{\kappa_1-1})$.
 - 4: **Step 2:** Find $(\Upsilon_{\kappa_1}, \rho_{\kappa_1}, \tau_{\kappa_1}, \theta_{\kappa_1})$ by solving (29) for a given $(\mathbf{p}_{\kappa_1}, \phi_{\kappa_1}, \mathbf{r}_{\kappa_1}^{\text{FH}}, \mathbf{r}_{\kappa_1}^{\text{BH}})$.
 - 5: **Until** $|\bar{\$}_{\text{tot}}^{\text{LD}}(\kappa_1) - \bar{\$}_{\text{tot}}^{\text{LD}}(\kappa_1 - 1)| \leq \varepsilon_1$ or $\kappa_1 = \Gamma_1$.
 - 6: Set $\kappa_1 = \kappa_1 + 1$.
 - 7: **end for**
 - 8: $\Upsilon_{\kappa_1}, \rho_{\kappa_1}, \mathbf{p}_{\kappa_1}, \phi_{\kappa_1}, \mathbf{r}_{\kappa_1}^{\text{FH}}, \mathbf{r}_{\kappa_1}^{\text{BH}}, \tau_{\kappa_1}$, and θ_{κ_1} are adopted for the network.
-

A. DACPSs and Delivery Algorithm

Here, we propose an efficient solution algorithm for (29) by utilizing an alternative approach [7], [29], [33] which consists of two main steps: 1) finding joint $\mathbf{p}, \phi, \mathbf{r}^{\text{FH}}$ and \mathbf{r}^{BH} ; 2) finding joint Υ, ρ, τ and θ . We repeat the mentioned steps until we have $|\bar{\$}_{\text{tot}}^{\text{LD}}(\kappa_1) - \bar{\$}_{\text{tot}}^{\text{LD}}(\kappa_1 - 1)| \leq \varepsilon_1$ where ε_1 is a positive small value and κ_1 is the iteration index, or the number of main iterations exceeds a pre-defined threshold Γ_1 . The proposed approach is summarized in Algorithm 1.

1) *Step 1:* In the first step, we obtain $\mathbf{p}, \phi, \mathbf{r}^{\text{FH}}$ and \mathbf{r}^{BH} jointly, by solving the following subproblem for fixed Υ, ρ, τ and θ as

$$\max_{\phi, \mathbf{p}, \mathbf{r}^{\text{BH}}, \mathbf{r}^{\text{FH}}} \bar{\$}_{\text{tot}}^{\text{LD}} \quad (31a)$$

$$\text{s.t. (7)-(10), (14), (16), (21d), (22), (24), (29b).}$$

Problem (31) is still MINLP which is NP-hard, due to the non-convexity and non-concavity of the access data rate functions in (24), and both (31a) and (29b), respectively, fractional SINR function in (22), fractional delay functions in (14), (16) and (24), and combinatorial constraint (21d) with respect to ϕ . In order to deal with mentioned challenges, we first relax $\phi_b^{v_h, v_l}$ to be a non-negative real value [11], which can be applied well-known in this context since the maximum number of CPU cycles in each processor is on the order of 10^9 [10], [12]. For the non-convex constraints, we apply transformation methods to tackle their non-convexity (please see Appendix A). Then, to tackle the non-concavity of $\bar{r}_{b,u}^{\text{Ac}}$ in (31a) and (29b) and non-convexity

Algorithm 2 The proposed SCA algorithm with the D.C. approximation method

- 1: Initialize \mathbf{p}_0 .
 - repeat**
 - 2: Update the convex approximated forms of (29b), (34e)-(34i) and substitute them into (34).
 - 3: Find $(\phi_{\kappa_2}, \mathbf{p}_{\kappa_2}, \mathbf{r}_{\kappa_2}^{\text{BH}}, \mathbf{r}_{\kappa_2}^{\text{FH}})$ by solving the convex approximated problem of (34).
 - 4: Set $\kappa_2 = \kappa_2 + 1$
 - Until** Convergence of \mathbf{p} .
 - 5: The variables \mathbf{p} , \mathbf{r}^{BH} , \mathbf{r}^{FH} , and ϕ are the outputs of the algorithm.
-

of it in (34e)-(34i) in the transformed problem, we use the successive convex approximation (SCA) approach based on the difference-of-two-concave-functions (D.C.) approximation method [31], [33], [34]. In this regard, we first initialize the approximation parameters. Then, we solve the convex approximated problem to find $(\phi, \mathbf{p}, \mathbf{r}^{\text{BH}}, \mathbf{r}^{\text{FH}})$. These iterations are repeated until the stopping criterion is satisfied. The derivations of the proposed SCA algorithm is presented in Appendix B. Moreover, the pseudo code of the SCA algorithm with the D.C. approximation method is summarized in Algorithm 2.

2) *Step 2*: Here, we jointly find the binary variables Υ , ρ , θ and τ for the given $(\mathbf{p}, \phi, \mathbf{r}^{\text{FH}}, \mathbf{r}^{\text{BH}})$ by solving the following subproblem

$$\begin{aligned} \min_{\Upsilon, \rho, \theta, \tau} \quad & \bar{\$}_{\text{tot}}^{\text{LD}} \\ \text{s.t.} \quad & (1), (3), (4), (8)-(10), (14), (16), (21\text{b})-(21\text{d}), (22)-(24), (29\text{b}), (29\text{c}). \end{aligned} \quad (32\text{a})$$

(32) is classified as integer nonlinear programming (INLP) due to combinatorial constraints (21d) with respect to Υ , θ , and τ , combinatorial constraints in (29c) with respect to ρ , nonlinear SIC constraint (22) with respect to τ , the term $\min\{\sum_{u=1}^U \theta_{b,u}, 1\}$ in (23), both the terms $\max_{u \in \mathcal{U}_m}\{\tau_{b,u}^n\}$ and $\min\{\sum_{u \in \mathcal{U}_m} \theta_{b,u}, 1\}$ in (32a) (please refer to (27)), multiplication of $\min\{\sum_{u \in \mathcal{U}_m} \theta_{b,u}, 1\}$ in scheduling variables in Υ in (32a) (please refer to (27) and (19)), nonlinearity of fractional delay functions in (14) and (16), and average access delay functions in (24) with respect to τ . To solve (32), our aim is to transform (32) into an integer disciplined convex programming (IDCP) which can be easily solved by utilizing the efficient standard optimization software CVX with the internal solver MOSEK that applies the Branch&bound&cut algorithm [30], [34]–[36].

Proposition 1: The INLP problem (32) can be equivalently transformed into an IDCP form which is presented in Appendix C.

To solve (21) for phase 2, we can also apply Algorithm 1, since when ρ is fixed, (21) and (29) have the similar structure. Due to the space limitations, the solution of problem phase 2 is neglected. To solve (30) in the HD scheme, we again apply a similar method to Algorithm 1 (See Appendix D).

B. Convergence of The Proposed Algorithms

Here, we discuss the convergence of our proposed Algorithm 1 for solving (29). This discussion is presented in the format of the following two propositions.

Proposition 2: The objective function (29a) is upper-bounded by the total average reward of slices which is obtained by $\sum_{u \in \mathcal{U}_m} \sum_{b \in \mathcal{B}} \bar{r}_{b,u}^{\text{Ac}} \psi_m$ that is a nonnegative finite term, due to limited access bandwidth and constraint (7). Therefore, for a feasible problem (29), the proposed alternative Algorithm 1 will converge to a locally optimal solution.

Proof. Please see Appendix E. □

Proposition 3: The SCA approach with the D.C. approximation method generates a sequence of improved feasible solutions. Therefore, the proposed algorithm for solving (31) will converge to a locally optimal solution when the number of SCA iterations are large enough.

Proof. Please see Appendix F. □

Since all proposed algorithms have similar structures, the convergence of the other algorithms can be proved same as the proposed Algorithm 1 for solving (29).

C. Computational Complexity

Since the proposed alternative algorithms for solving (21), (29) and (30) have basically the same structure, we only present the computational complexity of solving (29) using Algorithm 1. The computational complexity of solving (21) and (30) can also be obtained as the same way of solving (29).

In the first step of Algorithm 1, we first use a transformation method presented in Appendix A to solve (31) and then, we solve the equivalent result problem (34) using the iterative SCA approach based on the D.C. approximation method. In each iteration κ_2 of SCA, the approximated

disciplined convex programming (DCP) problem of (34) is solved by CVX which employs the geometric programming with the interior-point method (IPM) [34], [35]. Therefore, the computational complexity of solving the approximated problem of (34) is on the order of $\Omega_{LD}^1 = \frac{\log(T_{LD}^1/(t^0 \varrho))}{\log \epsilon^0}$, where $T_{LD}^1 = 3B + B^2 + U + M + BU^2N + BVLU(1 + B + L) + B^2VL^2(2 + 2U)$ is the total number of constraints in the approximated problem of (34), t^0 is the initial point for approximating the accuracy of the IPM, $0 < \varrho \ll \infty$ is the stopping criterion for the IPM, and ϵ^0 is for updating the accuracy of the IPM [34], [35]. Note that Ω_{LD}^1 is only for one iteration of the SCA approach. The total complexity of solving (34) by using the SCA method mainly depends on the number of optimization variables, constraints and accuracy of the algorithm. At the second step of Algorithm 1, we find $(\Upsilon, \rho, \theta, \tau)$, by solving (32). In fact, we transform (32) into an equivalent IDCP problem (44) using the epigraph technique. The result IDCP problem (44) is also solved by utilizing CVX with the MOSEK solver. The complexity of solving (44) can thus be obtained by $\Omega_{LD}^2 = \frac{\log(T_{LD}^2/(t^0 \varrho))}{\log \epsilon^0}$, where $T_{LD}^2 = 3B + 2U + M + B^2 + 2BU + BN + 2BUN + BU^2N + BVL(2 + B + L + 6M + 4UN + 3LM + 3BM + 4LUN + 4BUN) + B^2VL^2(4 + 6M + 8UN)$ is the total number of constraints in (44). Accordingly, the total computational complexity of solving (29) is on the order of $\Omega_{LD}^{\text{tot}} = \Xi^{\text{Main}} (\Xi^{\text{SCA}} \Omega_{LD}^1 + \Omega_{LD}^2)$ where Ξ^{Main} and Ξ^{SCA} are the total number of main and SCA iterations, respectively.

The computational complexity of solving the cache placement optimization problem (30) can also be obtained as the same way of solving problem (29). In this line, the complexity of finding joint \mathbf{p} , ϕ , \mathbf{r}^{FH} and \mathbf{r}^{BH} at each iteration of the SCA approach is on the order of $\Omega_{HD}^1 = \frac{\log(T_{HD}^1/(t^0 \varrho))}{\log \epsilon^0}$, where T_{HD}^1 is exactly equal to T_{LD}^1 . On the other hand, the complexity of solving the second step of the proposed alternative algorithm for solving (30) is given by $\Omega_{HD}^2 = \frac{\log(T_{HD}^2/(t^0 \varrho))}{\log \epsilon^0}$, where $T_{HD}^2 = 3B + 2U + M + B^2 + BU + BN + 2BUN + BU^2N + BVL(2 + B + L + 6U + 4UN + 3LU + 3BU + 4LUN + 4BUN) + B^2VL^2(4 + 6U + 8UN)$.

The complexity of solving (21) can be obtained as the same way of obtaining the complexity of solving (29), since both the proposed algorithms have the same structure for a fixed ρ . In this way, the complexity of solving (21) and finding \mathbf{p} , ϕ , \mathbf{r}^{FH} and \mathbf{r}^{BH} is exactly on the order of Ω_{LD}^1 . Moreover, the computational complexity of finding (Υ, θ, τ) is obtained by $\Omega_{\text{Del}}^2 = \frac{\log(T_{\text{Del}}^2/(t^0 \varrho))}{\log \epsilon^0}$, where $T_{\text{Del}}^2 = 2B + 2U + M + B^2 + 2BU + BN + 2BUN + BU^2N + BVL(2 + B + L + 6M + 4UN + 3LM + 3BM + 4LUN + 4BUN) + B^2VL^2(4 + 6M + 8UN)$.

D. A Low-Complexity Resource Allocation Framework

It is very important that the central scheduler be fast enough to readopt the delivery policy in each time slot of Phase 2 based on the arrival instantaneous requests of users and CSI, specifically in realistic ultra dense 5G wireless networks with a larger number of unique videos. In this way, we aim to propose another RAF which has a lower computational complexity in each time slot of Phase 2 than that of the framework proposed in Fig. 2. The main part of the complexity of the proposed framework in Fig. 2 is caused by reallocating the radio resources as well as reassociating users to RRSs at each time slot of Phase 2 to readopt the access transmission strategy based on the arrival requests and CSI. However, some environments with higher large-scale fading heavily limit the flexibility of the user association process and degrade the effect of the wireless small-scale fading on the SINR at users. On the other hand, we aim to utilize the benefits of radio resource allocation and user association policies in the MC-NOMA system to improve the users data rates and correspondingly the users revenues. Thus, in this novel framework, we adopt the obtained radio resource allocation, i.e., transmit power and subcarrier allocation, and user association policies in Phase 1 to all time slots of Phase 2. Hence, the system only reallocates the processing, fronthaul and backhaul resources as well as the request scheduling at the beginning of each time slot of Phase 2 based on the arrival requests of users. Accordingly, in this framework, the LD and HD cache placement problems are exactly the same as (29) and (30) whereas the delivery optimization problem at each time slot of Phase 2 is formulated as

$$\begin{aligned} & \max_{\phi, \mathbf{r}^{\text{BH}}, \mathbf{r}^{\text{FH}}, \Upsilon} \$_{\text{tot}} \\ & \text{s.t. } (2), (3), (8)-(10), (12)-(18). \end{aligned} \quad (33a)$$

The optimization problem (33) is a MINLP which can be efficiently solved by utilizing an alternative algorithm in which (33) is divided into two subproblems as: 1) finding joint ϕ , \mathbf{r}^{BH} , and \mathbf{r}^{FH} ; 2) finding Υ . The problem of finding joint ϕ , \mathbf{r}^{BH} , and \mathbf{r}^{FH} is a linear programming (LP) and thus, the globally optimal solution can be found by utilizing the CVX software or the Lagrange dual method. On the other hand, the IDCP problem of finding Υ is solved by using the MOSEK solver.

The computational complexity of solving (33) can be obtained as the same way of obtaining the complexity of solving (21). In this way, the complexity of finding ϕ , \mathbf{r}^{BH} , and \mathbf{r}^{FH} is on

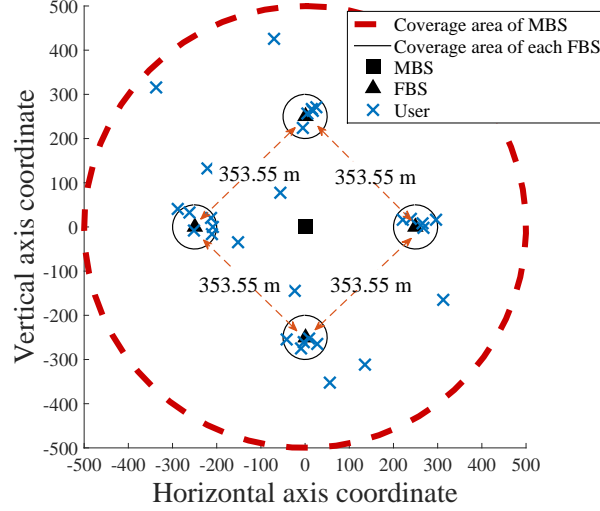


Fig. 4: Network setup and users placement in the simulation results.

the order of $\Omega_{\text{Del,LowComplex}}^1 = \frac{\log(T_{\text{Del,LowComplex}}^1 / (t^0 \varrho))}{\log \epsilon^0}$, where $T_{\text{Del,LowComplex}}^1 = 2B + B^2 + BVL(1 + B + L) + 4B^2VL^2$. Moreover, the complexity of finding Υ is obtained by $\Omega_{\text{Del,LowComplex}}^2 = \frac{\log(T_{\text{Del,LowComplex}}^2 / (t^0 \varrho))}{\log \epsilon^0}$, where $T_{\text{Del,LowComplex}}^2 = 2B + B^2 + BVL(3 + 2B + 2L) + 6B^2VL^2$.

IV. SIMULATION RESULTS

In this section, we present simulation results to demonstrate the performance of our proposed CPSs via MATLAB Monte Carlo simulations through 500 network realizations [14]. The network topology and user placement is shown in Fig. 4 where a single high-power RRS (HP-RRS), i.e., MBS, is located in a central of a circular area with radius 500 m and 4 low-power RRSs (LP-RRS), i.e., FBS, are located in a distance of 250 m from the HP-RRS⁷ [33]. 10 users are uniformly deployed in the coverage area of HP-RRS while 5 users are located in the coverage area of each LP-RRS with radii of 50 m [33]. As seen in Fig. 4, the shortest distance from a FBS to another FBS is $250\sqrt{2} \approx 353.55$ m.

The wireless channel is centered at a frequency of 2.5 GHz with bandwidth $W = 5$ MHz, $N = 64$ and $W_s = 78.125$ KHz [28]. The combined path loss and shadowing is modeled as $128.1 + 37.6 \log_{10} d_{b,u} + z_{b,u}$ in dB in which $z_{b,u}$ is a log-normal shadowing random variable with the standard deviation of 8 dB, and $d_{b,u} > 0$ denotes the distance between RRS b and user u in km [8], [29], [37]. The small-scale fading of the wireless channel is modeled as independent and

⁷We assume that RRS 1 is a HP-RRS while RRSs 2, ..., 5 are LP-RRSs.

identically distributed Rayleigh fading with variance 1 [29]. The CDI is averaged over 1000 CSI samples for a fixed channel power loss, since the location of users and RRSs are fixed in our numerical examples. The PSD of AWGN noise is set to $N_0 = -174$ dBm/Hz with a noise figure of 9 dB at each user [18]. In the MC-NOMA technology, we set $\Psi_b = 2, \forall b \in \mathcal{B}$ [28]–[30]. For the HP-RRS, we set $P_1^{\max} = 47$ dBm whereas for each LP-RRS b , $P_b^{\max} = 27$ dBm [33].

We assume that there exists $V = 10$ unique videos, each having $L = 4$ bitrate variants. In our simulations, we set the relative bitrates of the four variants to be 0.45, 0.55, 0.67, and 0.82 of the original video bitrate 2 Mbps (HD quality) [4], [5]. Besides, all video variants have equal length of 10 minutes [5]. The skew parameter of the Zipf distribution is set to $\lambda = 0.8$ [4], [5]. Similar to [4], [5] we assume that the processing workload η^{v_h, v_l} is proportional to s_{v_l} . In this regard, we set $\eta^{v_h, v_l} = s_{v_l}$ [5].

For the proposed virtualization model, we assume that there exists $M = 2$ slices in the infrastructure with $R_1^{\min} = 1$ Mbps and $R_2^{\min} = 2$ Mbps. Each slice also has $U/2 = 15$ users such that each user subscribes to any slices with a probability of $1/M = 50\%$ [13], [14]. In our proposed pricing scheme, we take $\mu_1^{\text{Cache}} = 2$ units/Gbit, $\mu_b^{\text{Cache}} = 1.6$ units/Gbit, $\forall b \in \mathcal{B}/\{1\}$, $\mu_1^{\text{Proc}} = 0.8$ units/GHz, $\mu_b^{\text{Proc}} = 0.7$ units/GHz, $\forall b \in \mathcal{B}/\{1\}$, $\alpha_1^{\text{Pow}} = 6$ units/Watt, $\alpha_b^{\text{Pow}} = 4$ units/Watt, $\forall b \in \mathcal{B}/\{1\}$, $\alpha_1^{\text{Sub}} = 60$ units/MHz, $\alpha_b^{\text{Sub}} = 40$ units/MHz, $\forall b \in \mathcal{B}/\{1\}$, $\alpha^{\text{FH}} = 2$ units/Mbps, $\alpha^{\text{BH}} = 5$ units/Mbps. Moreover, the unit reward of slices are $\psi_1 = 8.75$ units/Mbps and $\psi_2 = 9$ units/Mbps.

For processing capacities, we set $\chi_1^{\max} = 50$ GHz (maximum number of CPU cycles per seconds in HP-RRS is 50×10^9) and $\chi_b^{\max} = 25$ GHz, $\forall b \in \mathcal{B}/\{1\}$. Moreover, the required number of CPU cycles per byte at each RRS b is set to $N_{\text{Cycle}}^{v_h, v_l} = 5900$ [10], [38]. For the storage capacities, we set $C_1^{\max} = 0.2 \sum_{v_l \in \mathcal{V}} s_{v_l}$ and $C_b^{\max} = 0.1 \sum_{v_l \in \mathcal{V}} s_{v_l}, \forall b \in \mathcal{B}/\{1\}$. For the fronthaul and backhaul capacities, we set $R_{b',b}^{\max} = 40$ Mbps and $R_{0,b}^{\max} = 80$ Mbps, respectively. The simulation settings are summarized in Table II.

To investigate the benefits of each technology in the system, we compare the CVCT system with following schemes: 1) No Caching (NC) where the storage capacity of RRSs are equal to zero [18], [31]; 2) Non-Cooperative (NoCoop) where no cooperative caching as well as cooperative transcoding is considered for RRSs; 3) Cooperative Caching with No Transcoding (CCNT) where only the cooperative caching technology is considered for RRSs and the processing capacity of all RRSs are equal to zero; 4) The OMA technology (OMA) where the OFDMA technology is used for downlink of wireless access channels. We also compare the performance

TABLE II: Simulation settings.

Description	Notation	Value	Description	Notation	Value
System Parameters			Virtualization and Pricing Parameters		
Carrier frequency of wireless channel	\times	2.5 GHz	Number of slices	M	2
Wireless channel bandwidth	W	5 MHz	Number of users owned by each slice	\times	15
Number of subcarriers	N	64	User selection distribution	\times	Uniform
Subcarrier bandwidth	W_s	78.125 KHz	Unit price of transmit power	α_b^{Pow}	HP-RRS: 6 units/Watt, LP-RRS: 4 units/Watt
Large-scale fading model	\times	$128.1 + 37.6 \log_{10} d_{b,u} + z_{b,u}$ (dB), $d_{b,u}$ (Km)	Unit price of subcarrier bandwidth	α_b^{Sub}	HP-RRS: 60 units/MHz, LP-RRS: 40 units/MHz
Shadowing standard deviation	$z_{b,u}$	8 dB	Unit price of storage resources	μ_b^{Cache}	HP-RRS: 2 units/Gbit, LP-RRS: 1.6 units/Gbit
Small-scale fading model	\times	Rayleigh fading with variance 1	Unit price of processing resources	μ_b^{Proc}	HP-RRS: 0.8 units/GHz, LP-RRS: 0.7 units/GHz
AWGN noise density	N_0	-174 dBm/Hz	Unit price of fronthaul capacity	α^{FH}	2 units/Mbps
Noise figure at users	\times	9 dB	Unit price of backhaul capacity	α^{BH}	5 units/Mbps
Video Parameters			Unit reward of slices	ψ_m	$\psi_1 = 8.75$ units/Mbps and $\psi_2 = 9$ units/Mbps
Number of unique videos	V	10	Threshold Parameters		
Number of bitrate variants	L	4	Maximum power of each RRS	P_b^{max}	HP-RRS: 47 dBm, LP-RRS: 27 dBm
Original video bitrate	\times	2 Mbps (HD quality)	Maximum processing capacity of each RRS	χ_b^{max}	HP-RRS: 50 GHz, LP-RRS: 25 GHz
Relative bitrates	\times	[0.45, 0.55, 0.67, 0.82]	Storage capacity percentage of each RRS	C_b^{max}	HP-RRS: 20%, LP-RRS: 10%
Video length	\times	10 minutes	Maximum fronthaul capacity	$R_{f,b}^{\text{max}}$	40 Mbps
Zipf parameter	λ	0.8	Maximum backhaul capacity	$R_{o,b}^{\text{max}}$	80 Mbps
Task workload	$N_{\text{Cycle}}^{\text{v}, \text{v}_i}$	5900	Maximum number of users for each subcarrier at each RRS	Ψ_b	2
Size of transcoding task	$\eta^{\text{v}, \text{v}_i}$	s_{v_i}	Minimum data rate of each slice	R_m^{min}	$R_1^{\text{min}} = 1$ Mbps, $R_2^{\text{min}} = 2$ Mbps

of our proposed DACPSs in each scheme with two conventional baseline popular/bitrate CPSs as: 1) Most Popular Video (MPV) where each RRS caches the most popular videos until its storage is full [18], [31]; 2) High-Bitrate Video (HBV) where each RRS caches the high-bitrate variants of video files randomly, until its storage is full.

As noted previously, obtaining the globally optimal solution of each cache placement and delivery optimization problem via the exhaustive search method would take an unrealistically long time for $U = 30$, $N = 64$, $B = 5$, and $VL = 40$ [31]. Thus, we limit our simulations study to only evaluate the performance of our proposed solution algorithms. We also investigate the delivery performance gain achieved by each of our proposed RAF in terms of total delivery revenue of slices and computational complexity of the delivery algorithm.

A. Convergence of the Proposed Delivery Algorithms

Fig. 5 demonstrates the convergence of the proposed delivery algorithm for different CPSs. As shown, for all heuristic and the LD and HD strategies, the proposed delivery algorithm converge to stable values in maximum 6 iterations. In this figure, the dash lines refer to the upper-bound solutions when the algorithm converges. From Fig. 5, it can be seen that after 3 iterations, the proposed approach will achieve up to 95% of its upper-bound value for different CPSs which ensures us the proposed algorithm can be applied in practical scenarios in multiuser HV-MECs.

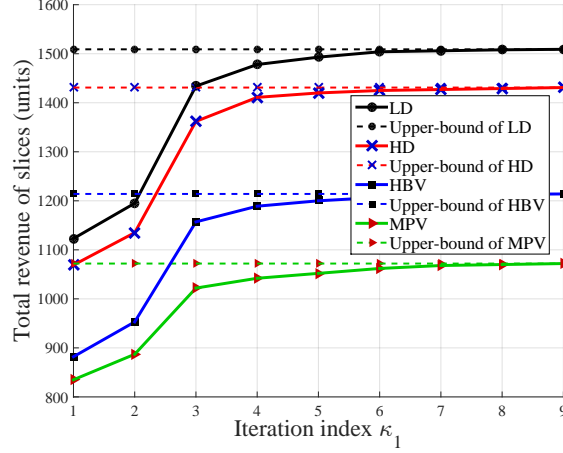
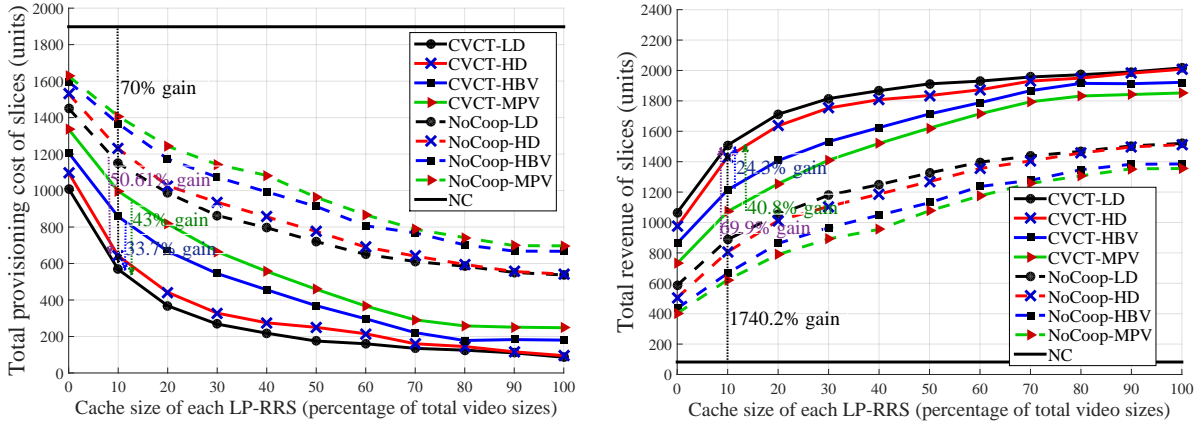


Fig. 5: The convergence in terms of total revenue of slices over the number of main iterations.

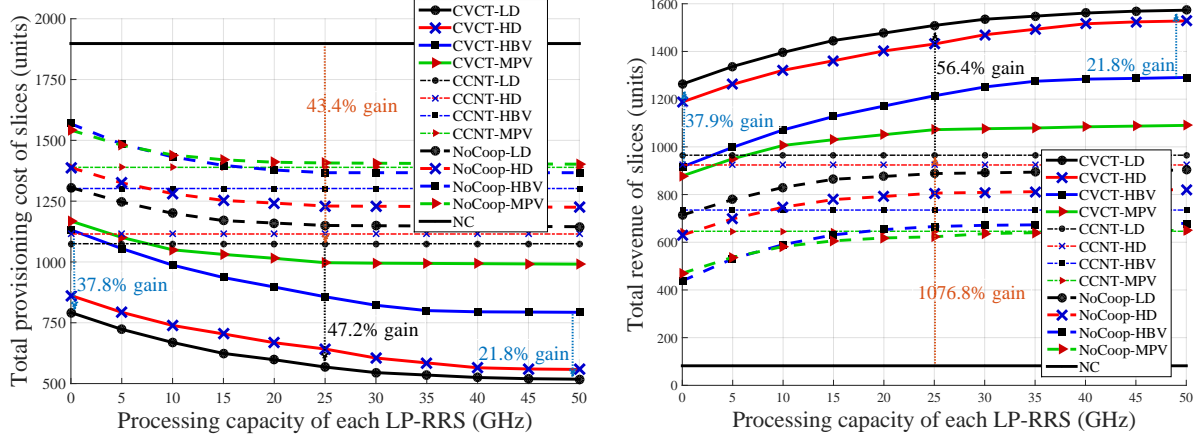


(a) Total provisioning cost of slices vs. storage capacity of LP-RRSs (b) Total revenue of slices vs. storage capacity of LP-RRSs

Fig. 6: Impact of storage capacity of LP-RRSs on the performance of CPSs in different schemes.

B. Impact of the Storage, Processing and Fronthaul Capacities

1) *Impact of the storage capacity of RRSs:* Fig. 6 investigates the impact of storage capacity limitation at LP-RRSs on the performance of CPSs in cooperative and non-cooperative schemes. As expected, more storage capacities lead to more storing videos which increases the cache hit ratio and subsequently provides more transcoding and cooperative communication opportunities. Therefore, the backhaul resource usage is significantly reduced, which degrades the total provisioning cost of slices (see Fig. 6(a)) and correspondingly increases the total revenue of slices which is shown in Fig. 6(b).



(a) Total provisioning cost of slices vs. processing capacity of LP-RRSs. (b) Total revenue of slices vs. processing capacity of LP-RRSs.

Fig. 7: Impact of processing capacity of LP-RRSs on the performance of CPSs in different schemes.

From Fig. 6(b), it is observed that the CVCT system has a huge performance gain in terms of total revenue of slices compared to the NC scheme. Actually, the NC scheme provides the upper-bound of total provisioning cost of slices (see Fig. 6(a)) which corresponds to the lower-bound of total revenue of slices. Specifically, for the LD strategy, the CVCT system degrades the total provisioning cost of slices nearly 70% compared to the NC scheme which correspondingly improves the total revenue of slices around 17-fold. On the other hand, the cooperation between RRSs degrades the total provisioning cost of slices around 50.61% compared to the NoCoop scheme. This reduction causes improving the total revenue of slices around 69.9%.

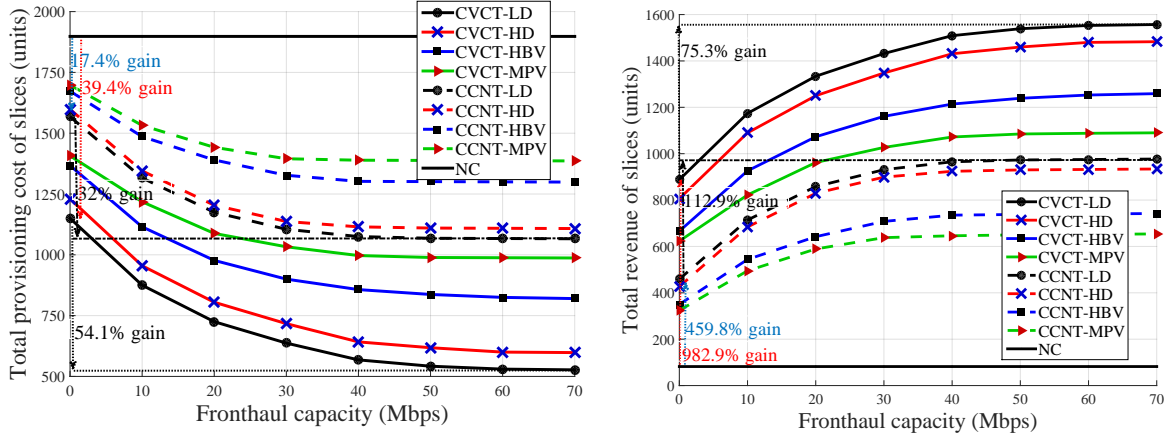
In these schemes for $\lambda = 0.8$, the LD strategy has higher performance than that of the HD strategy, specifically when the storage capacities are seriously limited. Besides, when the storage capacities are low, the HBV and MPV strategies have lower performances than those of our proposed LD and HD strategies, since they do not consider the flexible delivery opportunities. For instances, when the cache size percentage is equal to 10%, the LD strategy improves the total provisioning cost of slices up to 33.7% and 43% compared to the HBV and MPV strategies which improve the total revenue of slices around 24.3% and 40.8%, respectively.

2) *Impact of the processing capacity of RRSs:* Via Fig. 7, we investigate the impact of processing capacity limitation at LP-RRSs on the performance of CPSs in different schemes. Obviously, larger processing capacities provide more video transcoding opportunities which

alleviate the backhaul resource usage. Therefore, the total provisioning cost of slices decreases (see Fig. 7(a)) which improves the total revenue of slices that is shown in Fig. 7(b). It is noted that two transcoding types exist in the system as self-transcoding and cooperative transcoding. The self-transcoding in the parallel transmission and transcoding system mainly depends on the wireless channel, storage and processing capacities. In other words, for larger processing capacities, increasing them alone cannot significantly improve the self-transcoding opportunities, since the higher bitrate variants should be stored and the wireless channel capacities are limited. Besides, the cooperative transcoding mainly depends on the wireless channel, storage, processing and fronthaul link capacities. In other words, the cooperative transcoding operations cannot be successfully performed if there are no sufficient fronthaul capacities between RRSs. Accordingly, based on the available storage and fronthaul capacities, it can be seen that the performance of all CPSs have slow changes when the processing capacity of LP-RRSs exceed 35 GHz and 15 GHz for the CVCT and NoCoop schemes, respectively which is shown in Fig. 7.

From Fig. 7(a), for the LD strategy, there exists around 43.4% performance improvement in terms of total provisioning cost of slices by the CCNT scheme (cooperative caching technology) compared to that of NC. Correspondingly, this technology improves the total revenue of slices up to 10-fold which is shown in Fig. 7(b). Moreover, the cooperative transcoding technology improves the total provisioning cost of slices closed to 47.2% alone in the cooperative schemes, when the processing capacity of LP-RRSs are 25 GHz. Therefore, the total revenue of slices is incremented closed to 56.4% via the cooperative transcoding capability. These results show the efficiency of cooperative transcoding instead of storing multiple variants of a unique convertible file for the case that the storage capacities are too limited.

From Fig. 7, it can be seen that the HBV strategy has higher changes compared to the other CPSs. This is because, the HBV strategy is constructed only based on the bitrate variants in order to increase the transcoding opportunities. Moreover, the HBV strategy empirically increases the cooperative transcoding opportunities by randomly storing the most bitrate variant of videos. Interestingly, when the relative processing capacities increase, the performance gain between the HBV and LD strategies decreases from 37.9% to 21.8%, shown in Fig. 7(b). Therefore, the HBV strategy can be a good candidate, when the processing capacities are not limited. On the other hand, the MPV strategy has slow changes compared to the other CPSs, since it does not guarantee the transcoding of video files in the network. Moreover, MPV stores the same most popular videos which significantly degrades the cooperative communication opportunity in the



(a) Total provisioning cost of slices vs. fronthaul capacity between RRSs. (b) Total revenue of slices vs. fronthaul capacity between RRSs.

Fig. 8: Impact of fronthaul capacities between RRSs on performance of CPSs in different schemes.

system.

3) *Impact of the fronthaul capacity of RRSs:* Fig. 8 investigates the impact of the fronthaul capacity limitation between RRSs on the performance of CPSs in the CVCT and CCNT schemes. Generally, larger fronthaul capacities increase the cooperative communication capability in the system. Hence, larger values of $R_{b',b}^{\max}$ reduce the backhaul resource usage which corresponds degrading the total provisioning cost of slices in the cooperative system which is shown in Fig. 8(a). In this way, the total revenue of slices is improved (see Fig. 8(b)).

For the LD strategy, the total provisioning cost of slices in the CVCT scheme is decreased nearly 54.1% when $R_{b',b}^{\max}$ varies from zero, i.e., the NoCoop scheme, to 70 Mbps. Subsequently, this reduction improves the total revenue of slices closed to almost 75.3% which is caused by the CVCT scheme. As the same way, 32% performance gain in terms of the total provisioning cost of slices can be achieved in the CCNT scheme which improves the total revenue of slices nearby 112.9% that is caused only by the cooperative caching technology in the system. As seen in Fig. 8(a), the caching capability without any cooperation improves the total provisioning cost of slices nearly 17.4% compared to the NC scheme which causes nearby 459.8% improvement in the total revenue of slices. Moreover, the joint caching and transcoding capability at RRSs without any cooperation degrades the total provisioning cost of slices closed to almost 39.4% compared to the NC scheme which improves the systems delivery performance in terms of the total revenue of slices nearly 10-fold. From this result, it can be concluded that the self-transcoding capability

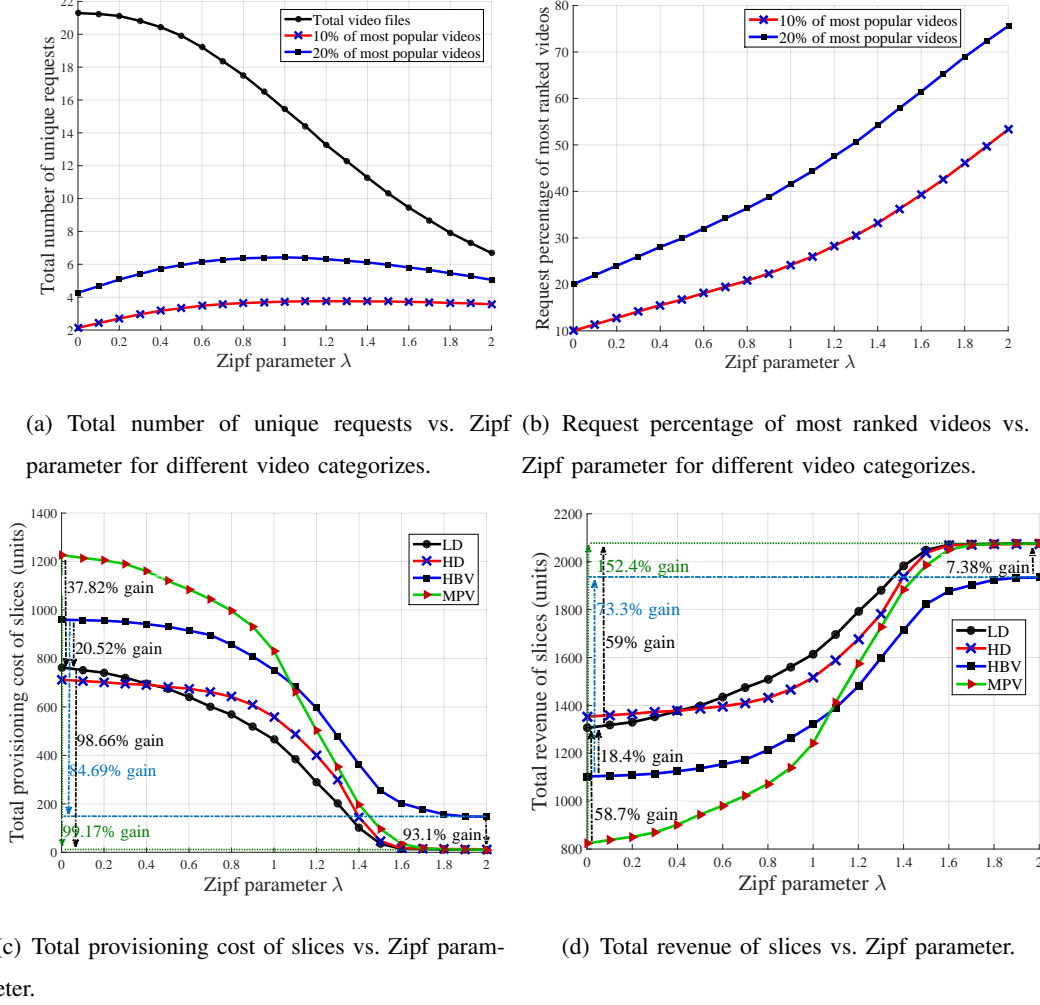


Fig. 9: Effect of the Zipf parameter on performance of different CPSs.

in the system improves the total revenue of slices up to 5-fold alone compared to the NC scheme.

C. Effect of Zipf Parameter

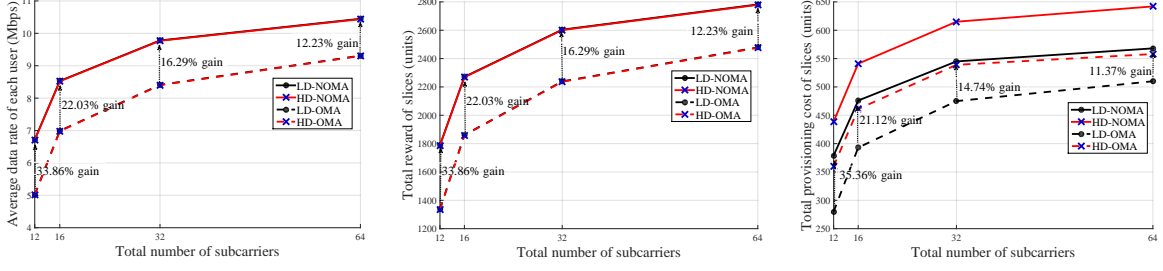
Fig. 9 investigates the effect of Zipf parameter λ on the performance of different CPSs. As shown in Fig. 9(a), for $\lambda = 1.5$, $U = 30$, and $VL = 40$, there is nearly 10.3 unique requests in the network in which closed to almost 5.97 and 3.74 unique requests are for 20% and 10% of most popular videos, respectively. This result is averaged over 10000 sets of requests. In other words, for this network settings, nearly 57.90% and 36.22% of unique requests are for 20% and 10% of most popular videos respectively which is shown in Fig. 9(b). Figs. 9(a) and 9(b) show that when λ increases, the diversity of requests of users degrades in the system.

Moreover, the request percentage of most ranked videos increases in the system, exponentially. In this regard, the backhaul, fronthaul, and processing resource usages are decreased in the network, significantly, which degrade the total provisioning cost of slices that is shown in Fig. 9(c). Subsequently, the total revenue of slices increases (see Fig. 9(d)).

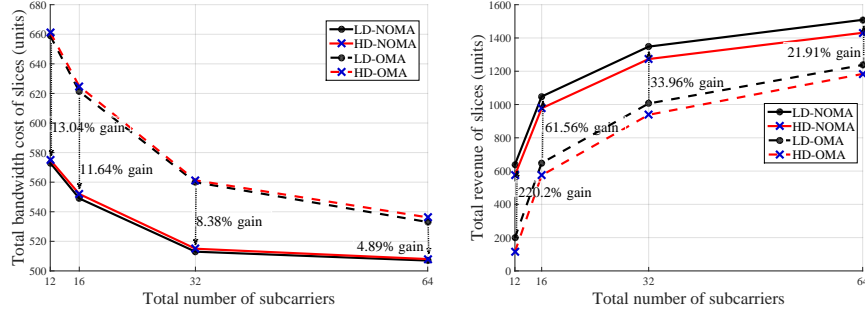
Based on Figs. 9(c) and 9(d), it can be derived that the HD strategy is more compatible than that of the LD strategy when λ tends to zero, i.e., when the diversity of requests increases. Besides, MPV is more affected by the Zipf parameter than that of other strategies, since it is only a baseline popular strategy. Actually, the total provisioning cost of slices by MPV is decreased nearly 99.17% which causes closed to almost 152.4% improvement in the total revenue of slices, when λ varies from 0 to 2. For $\lambda = 0$, i.e., when users uniformly request videos, the HBV strategy has more performance gain than that of MPV. In addition, the performance gaps in terms of the total revenue of slices between the LD and HBV strategies and the LD and MPV strategies are nearly 18.4% and 57.8%, respectively. These results show that MPV is not compatible for the system, when λ is too small, whereas HBV can be a good solution with its very low complexity. On the other hand, when λ is large enough, i.e., only a few popular videos are frequently requested by users through the network, the performance gaps between our strategies and MPV degrade significantly in the system. Actually, MPV is closed to almost the optimal strategy when λ is too large. It is noted that there still exists a performance gap (nearly 7.38% in terms of total revenue of slices) between HBV and other strategies when λ is too large, since HBV does not consider the popularity of videos in its algorithm structure.

D. Comparison Study Between MC-NOMA and OMA

Fig. 10 compares the performance of MC-NOMA and OMA in the LD and HD strategies for different values of total number of subcarriers N . Generally, increasing N in the multicarrier wireless networks improves the spectral efficiency at users. In this regard, the average data rate of users in the system increases which is shown in Fig. 10(a). This improvement causes an increment on the total reward of slices (see Fig. 10(b)). However, with increasing the data rate of users, more backhaul, fronthaul, and processing resources are required to satisfy access delay constraints (12), (13), (15), (17), and (18) in the parallel transmission and transcoding system. In this regard, the provisioning cost of slices increases which is shown in Fig. 10(c). Interestingly, with increasing N , the expensive bandwidth usages in the system degrade, significantly, which correspond decreasing the total bandwidth cost of slices (see Fig. 10(d)). This is due to the



(a) Average data rate of each user vs. total number of subcarriers. (b) Total reward of slices vs. total number of subcarriers. (c) Total provisioning cost of slices vs. total number of subcarriers.

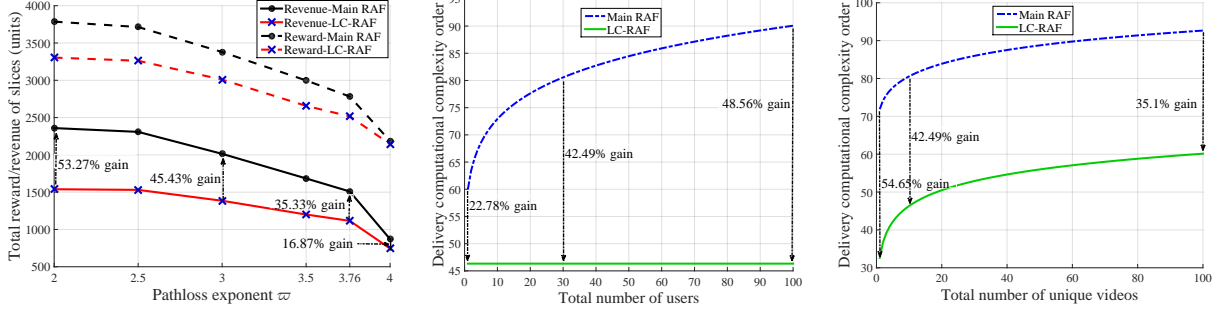


(d) Total bandwidth cost of slices vs. total number of subcarriers. (e) Total revenue of slices vs. total number of subcarriers.

Fig. 10: Effect of the total number of subcarriers on performance of the LD and HD strategies in the MC-NOMA and OMA schemes.

fact that the flexibility of subcarrier allocation in the multicarrier system is improved when N increases. Hence, more opportunities are provided for slices to assign the available subcarriers to the users and satisfy the QoS requirements. The bandwidth cost reduction and slices rewards increments both together more affects the revenue of slices than the increment of the provisioning costs. Hence, increasing N improves the total revenue of slices which is shown in Fig. 10(e).

MC-NOMA is expected to increase the spectral efficiency more than OMA by performing SIC at receivers. This result is shown in Fig. 10(a) in terms of users data rates. In this regard, the total reward of slices are improved in the system (see Fig. 10(b)). Although MC-NOMA causes more provisioning costs than that of OMA because of increasing access data rates (see Fig. 10(c)), it degrades the total bandwidth cost of slices much more than OMA, since each slice can use the same subcarriers for its own users in each cell, while the price of each subcarrier bandwidth is paid once in that cell (see Equ. (20)). It is noted that this opportunity can only be arisen by the MC-NOMA technology, since it provides the reuse of orthogonal subcarriers at



(a) Total reward/revenue of slices vs. pathloss exponent ϖ . (b) Delivery computational complexity order vs. total number of users. (c) Delivery computational complexity order vs. total number of unique videos. In this simulation, we set $t^0 = 1$, $\rho = 1$ and $\epsilon^0 = e$. Moreover, we consider 3 iterations for both Algorithm 1 and the SCA approach.

Fig. 11: Performance comparison of our proposed RAFs in terms of total revenue of slices and computational complexity of the delivery algorithm for the LD strategy.

each RRS. As shown in Fig. 10(a), for $N = 12$, the average data rate of each user in MC-NOMA is nearly 33.86% improved compared to OMA. This performance gap is reduced to 12.23% when $N = 64$. This is because OMA with a seriously low number of subcarriers degrades the systems performance, since the flexibility of the bandwidth reusing in each cell are completely eliminated. According to Figs. 10(a) and 10(b), the performance gaps between OMA and MC-NOMA is the same for users data rates and rewards, since the reward of slices are directly proportional to the access data rate of users. From Fig. 10(d), it can be seen that for $N = 12$, MC-NOMA improves the total bandwidth cost of slices 13.04% compared to OMA and this reduction achieves to 4.98%, when $N = 64$. Finally, MC-NOMA improves nearly 220.2% the total revenue of slices compared to OMA, when $N = 12$, and this result is reduced to 21.91% when $N = 64$.

E. Comparison Study Between Our Proposed Resource Allocation Frameworks

Fig. 11 investigates the performance of our proposed LC-RAF compared to that of proposed in Fig. 2 in terms of total revenue of slices and the delivery computational complexity order. In Fig. 11(a) we assume that the large-scale fading is modeled as $128.1 + 10\varpi \log_{10}(d_{b,u}) + z_{b,u}$ in dB, where the path loss exponent ϖ varies from 2 to 4. Obviously, when ϖ increases, the data rate of users decrease in the system. Accordingly, the total reward of slices degrades which

reduces the total revenue of slices. Interestingly, as seen in Fig. 11(a), the performance gap between the main and low-complexity frameworks degrades from 53.27% to 16.87% when ϖ varies from 2 to 4. This is because, for larger values of ϖ , the flexibility of the user association process as well as the effect of the variations of small-scale fading degrade in the network. In this regard, users are more restricted and each user is associated to the RRS which provides high data rate for that user instead of choosing the RRS which has the requested video. On the other hand, the CVCT system can significantly compensate this restriction to prevent the increment of backhaul traffic. From Fig. 11(a), it can be observed that our proposed LC-RAF is a good solution for environments with larger values of ϖ .

As can be seen in Figs. 11(b) and 11(c), the computational complexity of the delivery algorithm in the LC-RAF is reduced closed to almost 48.56% and 35.1%, when the total number of users U and unique videos V are large enough, respectively. Interestingly, the complexity of the delivery algorithm in the LC-RAF does not depend on the number of users which is shown in Fig. 11(b). Therefore, this framework can be a good choice for dense environments.

V. CONCLUDING REMARKS

In this paper, we investigated the idea of developing a DACPS in a parallel CVCT system followed by a limited backhaul and fronthaul MC-NOMA-assisted HV-MEC. In this network, we first proposed a RAF based on the network operational time. In Phase 1, we designed two diversity-based schemes where in each scheme, we maximized the estimated average revenue of slices subject to the minimum required access data rate of each user owned by each slice and some systems fundamental constraints. In order to find an efficient solution for these large-scale and NP-hard problems, we proposed low-complexity alternative algorithms. To reduce the computational complexity of the delivery algorithm, we proposed a LC-RAF, where the radio resource allocation policy obtained in Phase 1 is adopted for all time slots of Phase 2. In numerical assessments, we showed that our DACPSs improve the average systems delivery cost significantly, compared to the conventional baseline bitrate/popular video CPSs, specifically in the cooperative schemes. Moreover, we showed that our proposed LC-RAF can be a good choice for dense environments with higher levels of large-scale fading.

APPENDIX A

EQUIVALENT TRANSFORMATION OF (31)

The optimization problem (31) can be transformed into the following equivalent form as

$$\max_{\phi, \mathbf{p}, \mathbf{r}^{\text{BH}}, \mathbf{r}^{\text{FH}}} \bar{\$}_{\text{tot}}^{\text{LD}} \quad (34\text{a})$$

s.t. (7)-(10), (21d), (29b),

$$\mathbb{E}_{\mathbf{h}} \left\{ h_{b,u}^n \left(I_{b,u'}^{\text{Intra},n} + I_{b,u'}^{\text{Inter},n} + \sigma_{b,u'}^n \right) \right\} > \mathbb{E}_{\mathbf{h}} \left\{ h_{b,u'}^n \left(\sum_{\substack{v \in \mathcal{U}, v \neq u' \\ h_{b,v}^n > h_{b,u'}^n}} p_{b,v}^n h_{b,u}^n + I_{b,u}^{\text{Inter},n} + \sigma_{b,u}^n \right) \right\},$$

$$\forall b \in \mathcal{B}, u, u' \in \mathcal{U}, n \in \mathcal{N}, \tau_{b,u}^n, \tau_{b,u'}^n > 0, \mathbb{E}_{\mathbf{h}} \{ h_{b,u}^n \} > \mathbb{E}_{\mathbf{h}} \{ h_{b,u'}^n \}, \quad (34\text{b})$$

$$t_{b',b}^{v_h, v_l} \frac{r_{b',b}^{v_l}}{s_{v_l}} \leq t_{b',b}^{v_h, v_l} \frac{\phi_{b'}^{v_h, v_l}}{\eta^{v_h, v_l} N_{\text{Cycle}}^{v_h, v_l}}, \quad (34\text{c})$$

$$w_{b',b}^{v_h, v_l} \frac{\phi_b^{v_h, v_l}}{\eta^{v_h, v_l} N_{\text{Cycle}}^{v_h, v_l}} \leq w_{b',b}^{v_h, v_l} \frac{r_{b',b}^{v_h}}{s_{v_h}}, \quad (34\text{d})$$

$$y_b^{v_h, v_l} \frac{\bar{r}_{b,u}^{\text{Ac}}}{s_{v_l}} \leq \frac{\phi_b^{v_h, v_l}}{\eta^{v_h, v_l} N_{\text{Cycle}}^{v_h, v_l}} y_b^{v_h, v_l}, \quad (34\text{e})$$

$$z_{b',b}^{v_l} \bar{r}_{b,u}^{\text{Ac}} \leq r_{b',b}^{v_l} z_{b',b}^{v_l}, \quad (34\text{f})$$

$$t_{b',b}^{v_h, v_l} \bar{r}_{b,u}^{\text{Ac}} \leq t_{b',b}^{v_h, v_l} r_{b',b}^{v_l}, \quad (34\text{g})$$

$$w_{b',b}^{v_h, v_l} \frac{\bar{r}_{b,u}^{\text{Ac}}}{s_{v_l}} \leq w_{b',b}^{v_h, v_l} \frac{\phi_b^{v_h, v_l}}{\eta^{v_h, v_l} N_{\text{Cycle}}^{v_h, v_l}}, \quad (34\text{h})$$

$$o_b^{v_l} \bar{r}_{b,u}^{\text{Ac}} \leq o_b^{v_l} r_{0,b}^{v_l}, \quad (34\text{i})$$

$$\phi_b^{v_h, v_l} \geq 0. \quad (34\text{j})$$

In this line, to tackle the fractional constraints (14), (16), and (24), we transform them into equivalent forms, respectively as (34c)-(34i). Note that (34e)-(34i) hold even $\bar{r}_{b,u}^{\text{Ac}} = 0$, i.e., user u is not connected to RRS b . We also note that in this transformation, (34c) and (34d) are turned into linear forms (with relaxed $\phi_b^{v_h, v_l}$). Constraints (22), (29b), and (34e)-(34i) are in non-convex forms due to the fractional form of SINR function $\gamma_{b,u}^n$, non-concavity and non-convexity of $\bar{r}_{b,u}^{\text{Ac}}$, respectively. However, (22) can be transformed into an equivalent linear form with respect to \mathbf{p} as (34b) meaning that (22) should be held when $\tau_{b,u}^n \tau_{b,u'}^n \neq 0$.

APPENDIX B

THE PROPOSED SCA ALGORITHM FOR SOLVING (34)

To tackle the non-convexity of both (34a) and (29b) and all constraints in (34e)-(34i), the access data rate function $\bar{r}_{b,u}^{\text{Ac}}$ should be transformed into concave and convex forms, respectively. To approximate the access data rate function $\bar{r}_{b,u}^{\text{Ac}}$ in (34a) and (29b) to a concave format at each iteration κ_2 of the SCA algorithm, we first define

$$r_{b,u}^n = f_{b,u}^n - g_{b,u}^n, \quad (35)$$

where $f_{b,u}^n$ and $g_{b,u}^n$ are concave functions with respect to \mathbf{p} . Moreover, $f_{b,u}^n$ and $g_{b,u}^n$ are formulated, respectively, by

$$f_{b,u}^n = \tau_{b,u}^n W_s \log_2 \left(I_{b,u}^{\text{Intra},n} + I_{b,u}^{\text{Inter},n} + \sigma_{b,u}^n + p_{b,u}^n h_{b,u}^n \right), \quad (36)$$

$$g_{b,u}^n = \tau_{b,u}^n W_s \log_2 \left(I_{b,u}^{\text{Intra},n} + I_{b,u}^{\text{Inter},n} + \sigma_{b,u}^n \right). \quad (37)$$

Then, we approximate $g_{b,u}^n(\mathbf{p}_{\kappa_2})$ at each iteration κ_2 by its first order Taylor series approximation around \mathbf{p}_{κ_2-1} as follows [33], [34]:

$$g_{b,u}^n(\mathbf{p}_{\kappa_2}) \approx g_{b,u}^n(\mathbf{p}_{\kappa_2-1}) + \nabla g_{b,u}^n(\mathbf{p}_{\kappa_2-1})(\mathbf{p}_{\kappa_2} - \mathbf{p}_{\kappa_2-1}), \quad (38)$$

where $\nabla g_{b,u}^n(\mathbf{p}_{\kappa_2-1})$ is a vector of length UB and its entry is obtained by

$$\nabla g_{b,u}^n(\mathbf{p}) = \begin{cases} 0, & \forall i = b, u' \in \mathcal{U}/\{u\}, h_{b,u'}^n \leq h_{b,u}^n; \\ \frac{\tau_{b,u}^n W_s h_{b,u}^n}{(\ln 2)(I_{b,u}^{\text{Intra},n} + I_{b,u}^{\text{Inter},n} + \sigma_{b,u}^n)}, & \forall i = b, u' \in \mathcal{U}/\{u\}, h_{b,u'}^n > h_{b,u}^n; \\ \frac{\tau_{b,u}^n W_s h_{i,u}^n}{(\ln 2)(I_{b,u}^{\text{Intra},n} + I_{b,u}^{\text{Inter},n} + \sigma_{b,u}^n)}, & \forall i \neq b, u' \in \mathcal{U}/\{u\}. \end{cases} \quad (39)$$

Therefore, the concave approximated function of $\bar{r}_{b,u}^n$ at each iteration κ_2 is expressed by

$$\hat{r}_{b,u}^n(\mathbf{p}_{\kappa_2}) \approx \mathbb{E}_{\mathbf{h}} \left\{ f_{b,u}^n(\mathbf{p}_{\kappa_2}) - g_{b,u}^n(\mathbf{p}_{\kappa_2-1}) - \nabla g_{b,u}^n(\mathbf{p}_{\kappa_2-1})(\mathbf{p}_{\kappa_2} - \mathbf{p}_{\kappa_2-1}) \right\}. \quad (40)$$

Besides, in order to approximate $\bar{r}_{b,u}^{\text{Ac}}$ in (34e)-(34i) to a convex form at each iteration κ_2 of the SCA algorithm, we first define $\bar{r}_{b,u}^{\text{Ac}}$ as a D.C. function in (35). Then, we approximate $f_{b,u}^n(\mathbf{p}_{\kappa_2})$ at each iteration κ_2 by its first order Taylor series approximation around \mathbf{p}_{κ_2-1} as

$$f_{b,u}^n(\mathbf{p}_{\kappa_2}) \approx f_{b,u}^n(\mathbf{p}_{\kappa_2-1}) + \nabla f_{b,u}^n(\mathbf{p}_{\kappa_2-1})(\mathbf{p}_{\kappa_2} - \mathbf{p}_{\kappa_2-1}), \quad (41)$$

where $\nabla f_{b,u}^n(\mathbf{p}_{\kappa_2-1})$ is a vector of length UB and its entry is expressed by

$$\nabla f_{b,u}^n(\mathbf{p}) = \begin{cases} \frac{\tau_{b,u}^n W_s h_{b,u}^n}{(\ln 2)(I_{b,u}^{\text{Intra},n} + I_{b,u}^{\text{Inter},n} + \sigma_{b,u}^n + p_{b,u}^n h_{b,u}^n)}, & \forall i = b, u' = u; \\ 0, & \forall i = b, u' \in \mathcal{U}/\{u\}, h_{b,u'}^n \leq h_{b,u}^n; \\ \frac{\tau_{b,u}^n W_s h_{b,u}^n}{(\ln 2)(I_{b,u}^{\text{Intra},n} + I_{b,u}^{\text{Inter},n} + \sigma_{b,u}^n + p_{b,u}^n h_{b,u}^n)}, & \forall i = b, u' \in \mathcal{U}/\{u\}, h_{b,u'}^n > h_{b,u}^n; \\ \frac{\tau_{b,u}^n W_s h_{i,u}^n}{(\ln 2)(I_{b,u}^{\text{Intra},n} + I_{b,u}^{\text{Inter},n} + \sigma_{b,u}^n + p_{b,u}^n h_{b,u}^n)}, & \forall i \neq b, u' \in \mathcal{U}/\{u\}. \end{cases} \quad (42)$$

Hence, the convex approximated form of $\bar{r}_{b,u}^n$ at each iteration κ_2 is given by

$$\tilde{r}_{b,u}^n(\mathbf{p}_{\kappa_2}) \approx \mathbb{E}_{\mathbf{h}} \left\{ f_{b,u}^n(\mathbf{p}_{\kappa_2-1}) + \nabla f_{b,u}^n(\mathbf{p}_{\kappa_2-1})(\mathbf{p}_{\kappa_2} - \mathbf{p}_{\kappa_2-1}) - g_{b,u}^n(\mathbf{p}_{\kappa_2}) \right\}. \quad (43)$$

By substituting $\hat{r}_{b,u}^n$ in (34a) and (29b) and $\tilde{r}_{b,u}^n$ in (34e)-(34i), the optimization problem (34) is transformed into an approximated DCP form which can be easily solved by utilizing efficient convex programming solutions, such as the Lagrange dual method or the CVX software [11], [30], [35], [39], [40].

APPENDIX C

EQUIVALENT TRANSFORMATION OF (32)

The result IDCP form of (32) is formulated as

$$\min_{\mathbf{r}, \rho, \theta, \tau, \vartheta, \hat{\vartheta}, \nu, \hat{\mathbf{r}}, \check{\mathbf{r}}} \sum_{m \in \mathcal{M}} \bar{\$}_m^{\text{slice, Epi, 2}} \quad (44a)$$

s.t. (1), (3), (4), (8)-(10), (21b)-(21d), (25), (29b), (29c), (34c), (34d),

$$\frac{\mathbb{E}_{\mathbf{h}} \left\{ \sum_{n=1}^N \check{y}_{b,u}^{v_h, v_l, n} W_s \log_2(1 + \gamma_{b,u}^n) \right\}}{s_{v_l}} \leq \frac{\phi_b^{v_h, v_l}}{\eta^{v_h, v_l} N_{\text{Cycle}}^{v_h, v_l}} y_b^{v_h, v_l}, \forall u \in \mathcal{U}_m, \quad (44b)$$

$$\mathbb{E}_{\mathbf{h}} \left\{ \sum_{n=1}^N \check{z}_{b',b,u}^{v_l, n} W_s \log_2(1 + \gamma_{b,u}^n) \right\} \leq r_{b',b}^{v_l} z_{b',b}^{v_l}, \forall u \in \mathcal{U}_m, \quad (44c)$$

$$\frac{\mathbb{E}_{\mathbf{h}} \left\{ \sum_{n=1}^N \check{t}_{b',b,u}^{v_h, v_l, n} W_s \log_2(1 + \gamma_{b,u}^n) \right\}}{s_{v_l}} \leq t_{b',b}^{v_h, v_l} r_{b',b}^{v_l}, \forall u \in \mathcal{U}_m, \quad (44d)$$

$$\frac{\mathbb{E}_{\mathbf{h}} \left\{ \sum_{n=1}^N \check{w}_{b',b,u}^{v_h, v_l, n} W_s \log_2(1 + \gamma_{b,u}^n) \right\}}{s_{v_l}} \leq w_{b',b}^{v_h, v_l} \frac{\phi_b^{v_h, v_l}}{\eta^{v_h, v_l} N_{\text{Cycle}}^{v_h, v_l}}, \forall u \in \mathcal{U}_m, \quad (44e)$$

$$\mathbb{E}_{\mathbf{h}} \left\{ \sum_{n=1}^N \check{o}_{b,u}^{v_l, n} W_s \log_2(1 + \gamma_{b,u}^n) \right\} \leq o_b^{v_l} r_{0,b}^{v_l}, \forall u \in \mathcal{U}_m, \quad (44f)$$

$$\mathbb{E}_{\mathbf{h}} \left\{ \tau_{b,u}^n \frac{p_{b,u}^n h_{b,u}^n}{\sum_{\substack{v \in \mathcal{U}, v \neq u' \\ h_{b,v}^n > h_{b,u}^n}} p_{b,v}^n h_{b,u}^n + I_{b,u}^{\text{Inter},n} + \sigma_{b,u}^n} \right\} > \mathbb{E}_{\mathbf{h}} \{ \tau_{b,u}^n \gamma_{b,u'}^n \}, \forall b \in \mathcal{B}, u, u' \in \mathcal{U}, n \in \mathcal{N},$$

$$p_{b,u}^n, p_{b,u'}^n > 0, \mathbb{E}_{\mathbf{h}} \{ h_{b,u}^n \} > \mathbb{E}_{\mathbf{h}} \{ h_{b,u'}^n \}, \quad (44\text{g})$$

$$\vartheta_b \geq \theta_{b,u}, \forall b \in \mathcal{B}, u \in \mathcal{U}, \quad \vartheta_b \in \{0, 1\}, \quad (44\text{h})$$

$$x_b^{v_l} + \sum_{\substack{v_h \in \mathcal{V} \\ h > l}} y_b^{v_h, v_l} + \sum_{\substack{b' \in \mathcal{B} \\ b' \neq b}} z_{b',b}^{v_l} + \sum_{\substack{b' \in \mathcal{B} \\ b' \neq b}} \sum_{\substack{v_h \in \mathcal{V} \\ h > l}} (t_{b',b}^{v_h, v_l} + w_{b',b}^{v_h, v_l}) + o_b^{v_l} = \vartheta_b, \forall b \in \mathcal{B}, v_l \in \mathcal{V}, \quad (44\text{i})$$

$$\tilde{\vartheta}_{b,m} \geq \theta_{b,u}, \forall b \in \mathcal{B}, u \in \mathcal{U}_m, \quad \tilde{\vartheta}_{b,m} \in \{0, 1\}, \quad (44\text{j})$$

$$\nu_{b,m}^n \geq \tau_{b,u}^n, \forall b \in \mathcal{B}, n \in \mathcal{N}, u \in \mathcal{U}_m, \quad \nu_{b,m}^n \in \{0, 1\}, \quad (44\text{k})$$

$$\hat{x}_{b,m}^{v_l} \leq x_b^{v_l}, \quad \hat{x}_{b,m}^{v_l} \leq \tilde{\vartheta}_{b,m}, \quad \hat{x}_{b,m}^{v_l} \geq x_b^{v_l} + \tilde{\vartheta}_{b,m} - 1, \quad \hat{x}_{b,m}^{v_l} \in \{0, 1\}, \quad (44\text{l})$$

$$\hat{y}_{b,m}^{v_h, v_l} \leq y_b^{v_h, v_l}, \quad \hat{y}_{b,m}^{v_h, v_l} \leq \tilde{\vartheta}_{b,m}, \quad \hat{y}_{b,m}^{v_h, v_l} \geq y_b^{v_h, v_l} + \tilde{\vartheta}_{b,m} - 1, \quad \hat{y}_{b,m}^{v_h, v_l} \in \{0, 1\}, \quad (44\text{m})$$

$$\hat{z}_{b',b,m}^{v_l} \leq z_{b',b}^{v_l}, \quad \hat{z}_{b',b,m}^{v_l} \leq \tilde{\vartheta}_{b,m}, \quad \hat{z}_{b',b,m}^{v_l} \geq z_{b',b}^{v_l} + \tilde{\vartheta}_{b,m} - 1, \quad \hat{z}_{b',b,m}^{v_l} \in \{0, 1\}, \quad (44\text{n})$$

$$\hat{t}_{b',b,m}^{v_h, v_l} \leq t_{b',b}^{v_h, v_l}, \quad \hat{t}_{b',b,m}^{v_h, v_l} \leq \tilde{\vartheta}_{b,m}, \quad \hat{t}_{b',b,m}^{v_h, v_l} \geq t_{b',b}^{v_h, v_l} + \tilde{\vartheta}_{b,m} - 1, \quad \hat{t}_{b',b,m}^{v_h, v_l} \in \{0, 1\}, \quad (44\text{o})$$

$$\hat{w}_{b',b,m}^{v_h, v_l} \leq w_{b',b}^{v_h, v_l}, \quad \hat{w}_{b',b,m}^{v_h, v_l} \leq \tilde{\vartheta}_{b,m}, \quad \hat{w}_{b',b,m}^{v_h, v_l} \geq w_{b',b}^{v_h, v_l} + \tilde{\vartheta}_{b,m} - 1, \quad \hat{w}_{b',b,m}^{v_h, v_l} \in \{0, 1\}, \quad (44\text{p})$$

$$\hat{o}_{b,m}^{v_l} \leq o_b^{v_l}, \quad \hat{o}_{b,m}^{v_l} \leq \tilde{\vartheta}_{b,m}, \quad \hat{o}_{b,m}^{v_l} \geq o_b^{v_l} + \tilde{\vartheta}_{b,m} - 1, \quad \hat{o}_{b,m}^{v_l} \in \{0, 1\}, \quad (44\text{q})$$

$$\check{y}_{b,u}^{v_h, v_l, n} \leq y_b^{v_h, v_l}, \quad \check{y}_{b,u}^{v_h, v_l, n} \leq \tau_{b,u}^n, \quad \check{y}_{b,u}^{v_h, v_l, n} \geq y_b^{v_h, v_l} + \tau_{b,u}^n - 1, \quad \check{y}_{b,u}^{v_h, v_l, n} \in \{0, 1\}, \quad (44\text{r})$$

$$\check{z}_{b',b,u}^{v_l, n} \leq z_{b',b}^{v_l}, \quad \check{z}_{b',b,u}^{v_l, n} \leq \tau_{b,u}^n, \quad \check{z}_{b',b,u}^{v_l, n} \geq z_{b',b}^{v_l} + \tau_{b,u}^n - 1, \quad \check{z}_{b',b,u}^{v_l, n} \in \{0, 1\}, \quad (44\text{s})$$

$$\check{t}_{b',b,u}^{v_h, v_l, n} \leq t_{b',b}^{v_h, v_l}, \quad \check{t}_{b',b,u}^{v_h, v_l, n} \leq \tau_{b,u}^n, \quad \check{t}_{b',b,u}^{v_h, v_l, n} \geq t_{b',b}^{v_h, v_l} + \tau_{b,u}^n - 1, \quad \check{t}_{b',b,u}^{v_h, v_l, n} \in \{0, 1\}, \quad (44\text{t})$$

$$\check{w}_{b',b,u}^{v_h, v_l, n} \leq w_{b',b}^{v_h, v_l}, \quad \check{w}_{b',b,u}^{v_h, v_l, n} \leq \tau_{b,u}^n, \quad \check{w}_{b',b,u}^{v_h, v_l, n} \geq w_{b',b}^{v_h, v_l} + \tau_{b,u}^n - 1, \quad \check{w}_{b',b,u}^{v_h, v_l, n} \in \{0, 1\}, \quad (44\text{u})$$

$$\check{o}_{b,u}^{v_l, n} \leq o_b^{v_l}, \quad \check{o}_{b,u}^{v_l, n} \leq \tau_{b,u}^n, \quad \check{o}_{b,u}^{v_l, n} \geq o_b^{v_l} + \tau_{b,u}^n - 1, \quad \check{o}_{b,u}^{v_l, n} \in \{0, 1\}, \quad (44\text{v})$$

where $\bar{\mathbf{S}}_m^{\text{slice}, \text{Epi}, 2} = \sum_{u \in \mathcal{U}_m} \sum_{b \in \mathcal{B}} \bar{r}_{b,u}^{\text{Ac}} \psi_m - \sum_{u \in \mathcal{U}_m} \sum_{b \in \mathcal{B}} \sum_{n \in \mathcal{N}} (p_{b,u}^n \alpha_b^{\text{Pow}}) - \sum_{b \in \mathcal{B}} \sum_{n \in \mathcal{N}} (\nu_{b,m}^n W_s \alpha_b^{\text{Sub}})$

$$- \sum_{b \in \mathcal{B}} \sum_{v_l \in \mathcal{V}} \Delta_{v_l} \left(\hat{x}_{b,m}^{v_l} (s_{v_l} \mu_b^{\text{Cache}}) + \sum_{\substack{v_h \in \mathcal{V} \\ h > l}} \hat{y}_{b,m}^{v_h, v_l} (s_{v_h} \mu_b^{\text{Cache}} + \phi_b^{v_h, v_l} \mu_b^{\text{Proc}}) + \sum_{\substack{b' \in \mathcal{B} \\ b' \neq b}} \hat{z}_{b',b,m}^{v_l} (s_{v_l} \mu_{b'}^{\text{Cache}} + r_{b',b}^{v_l} \alpha^{\text{FH}}) + \right.$$

$$\left. \sum_{\substack{b' \in \mathcal{B} \\ b' \neq b}} \sum_{\substack{v_h \in \mathcal{V} \\ h > l}} \hat{t}_{b',b,m}^{v_h, v_l} (s_{v_h} \mu_{b'}^{\text{Cache}} + \phi_{b'}^{v_h, v_l} \mu_{b'}^{\text{Proc}} + r_{b',b}^{v_l} \alpha^{\text{FH}}) + \sum_{\substack{b' \in \mathcal{B} \\ b' \neq b}} \sum_{\substack{v_h \in \mathcal{V} \\ h > l}} \hat{w}_{b',b,m}^{v_h, v_l} (s_{v_h} \mu_{b'}^{\text{Cache}} + r_{b',b}^{v_h} \alpha^{\text{FH}} + \right.$$

$$\left. \phi_b^{v_h, v_l} \mu_b^{\text{Proc}}) + \hat{o}_{b,m}^{v_l} (r_{0,b}^{v_l} \alpha^{\text{BH}}) \right), \quad \boldsymbol{\vartheta} = [\vartheta_b], \quad \tilde{\boldsymbol{\vartheta}} = [\tilde{\vartheta}_{b,m}], \quad \boldsymbol{\nu} = [\nu_{b,m}^n], \quad \hat{\mathbf{Y}} = [\hat{x}, \hat{y}, \hat{z}, \hat{t}, \hat{w}, \hat{o}],$$

$$\hat{\mathbf{x}} = [\hat{x}_{b,m}^{v_l}], \quad \hat{\mathbf{y}} = [\hat{y}_{b,m}^{v_h, v_l}], \quad \hat{\mathbf{z}} = [\hat{z}_{b',b,m}^{v_l}], \quad \hat{\mathbf{t}} = [\hat{t}_{b',b,m}^{v_h, v_l}], \quad \hat{\mathbf{w}} = [\hat{w}_{b',b,m}^{v_h, v_l}], \quad \hat{\mathbf{o}} = [\hat{o}_{b,m}^{v_l}], \quad \check{\mathbf{Y}} = [\check{y}, \check{z}, \check{t}, \check{w}, \check{o}],$$

$\check{\mathbf{y}} = [\check{y}_{b,u}^{v_h, v_l, n}]$, $\check{\mathbf{z}} = [\check{z}_{b',b,u}^{v_l, n}]$, $\check{\mathbf{t}} = [\check{t}_{b',b,u}^{v_h, v_l, n}]$, $\check{\mathbf{w}} = [\check{w}_{b',b,u}^{v_h, v_l, n}]$, and $\check{\mathbf{o}} = [\check{o}_{b,u}^{v_l, n}]$. In order to overcome the nonlinearity challenges in (32), we first transform (6) into an equivalent integer linear form in (44g) which should be held when $p_{b,u}^n, p_{b,u'}^n > 0$ and $h_{b,u}^n > h_{b,u'}^n$. In addition, by introducing a new binary variable ϑ_b , where

$$\vartheta_b \geq \theta_{b,u}, \forall b \in \mathcal{B}, \quad \vartheta_b \in \{0, 1\}, \quad (45)$$

(23) can be transformed into an equivalent form as (44i) which is in an integer linear form with respect to the new variable ϑ_b and all variables in Υ [41]. In the same line, by defining new variables $\tilde{\vartheta}_{b,m}$ and $\nu_{b,m}^n$ such that (44j) and (44k) are held, respectively, the term $\bar{\$}_m^{\text{slice,UB}}$ in (32a) is transformed into the following equivalent form as

$$\begin{aligned} \bar{\$}_m^{\text{slice,Epi,1}} = & \sum_{u \in \mathcal{U}_m} \sum_{b \in \mathcal{B}} \bar{r}_{b,u}^{\text{Ac}} \psi_m - \sum_{u \in \mathcal{U}_m} \sum_{b \in \mathcal{B}} \sum_{n \in \mathcal{N}} (p_{b,u}^n \alpha_b^{\text{Pow}}) - \sum_{b \in \mathcal{B}} \sum_{n \in \mathcal{N}} (\nu_{b,m}^n W_s \alpha_b^{\text{Sub}}) - \\ & \sum_{b \in \mathcal{B}} \tilde{\vartheta}_{b,m} \bar{\$}_b^{\text{Cost,RRS}}, \end{aligned} \quad (46)$$

which is still in the integer nonlinear form, because of binary bilinear products generated by multiplications of $\tilde{\vartheta}_{b,m}$ in all scheduling variables in Υ in the term $\tilde{\vartheta}_{b,m} \bar{\$}_b^{\text{Cost,RRS}}$. To handle this challenge, we utilize the following lemma to linearize each binary bilinear product.

Lemma 1. Assume that $x \in \{0, 1\}$ and $y \in \{0, 1\}$ are binary variables. The binary variable $z \in \{0, 1\}$ can be substituted with the binary bilinear product xy if $z \leq x$, $z \leq y$, and $z \geq x + y - 1$.

Proof. For each two binary variables x and y , the following equality is always satisfied: $xy = \min\{x, y\}$. By utilizing the epigraph technique and introducing a new binary variable $z \in \{0, 1\}$ such that $z \leq x$, $z \leq y$, and $z \geq x + y - 1$, the integer linear term z can be replaced with the integer nonlinear term xy . \square

Based on **Lemma 1**, by adding constraints (44l)-(44q), the binary variables $\hat{y}_{b,m}^{v_h, v_l}$, $\hat{z}_{b',b,m}^{v_l}$, $\hat{t}_{b',b,m}^{v_h, v_l}$, $\hat{w}_{b',b,m}^{v_h, v_l}$, and $\hat{o}_{b,m}^{v_l}$ are replaced with the binary bilinear products $y_b^{v_h, v_l} \tilde{\vartheta}_{b,m}$, $z_{b',b}^{v_l} \tilde{\vartheta}_{b,m}$, $t_{b',b}^{v_h, v_l} \tilde{\vartheta}_{b,m}$, $w_{b',b}^{v_h, v_l} \tilde{\vartheta}_{b,m}$, and $o_b^{v_l} \tilde{\vartheta}_{b,m}$ in (46), respectively, which turn (46) into a linear integer form.

To cope with nonlinearity of delay functions in (14) and (16), and average access delay functions in (24), we utilize the transformation method presented in Appendix A. To this end, we first transform (14) and (16) into (34c) and (34d), respectively, where both of them are in integer linear forms. Besides, we transform constraints in (24) into (34e)-(34i) which are still in integer nonlinear forms with respect to Υ and θ . According to **Lemma 1**, by adding

constraints (44r)-(44v), the binary variables $\check{y}_{b,u}^{v_h,v_l,n}$, $\check{z}_{b',b,u}^{v_l,n}$, $\check{t}_{b',b,u}^{v_h,v_l,n}$, $\check{w}_{b',b,u}^{v_h,v_l,n}$, and $\check{o}_{b,u}^{v_l,n}$ are replaced with the binary bilinear products $y_b^{v_h,v_l} \tau_{b,u}^n$, $z_{b',b}^{v_l} \tau_{b,u}^n$, $t_{b',b}^{v_h,v_l} \tau_{b,u}^n$, $w_{b',b}^{v_h,v_l} \tau_{b,u}^n$, and $o_b^{v_l} \tau_{b,u}^n$ in (34e)-(34i), respectively, where the result constraints (44b)-(44f) are in integer linear forms.

APPENDIX D

EQUIVALENT TRANSFORMATION OF (30)

The first step of Algorithm 1, i.e., finding joint \mathbf{p} , ϕ , \mathbf{r}^{FH} and \mathbf{r}^{BH} , is similar to the first step of solving (29) except that in the second step, i.e., finding joint Υ , ρ , τ and θ , $\theta_{b,u}$ is directly multiplied to all scheduling variables in Υ . Therefore, by using **Lemma 1**, (30) is transformed into an equivalent IDCP problem formulated as

$$\min_{\Upsilon, \rho, \theta, \tau, \vartheta, \nu, \check{\Upsilon}, \check{\Upsilon}} \sum_{m \in \mathcal{M}} \bar{\$}_m^{\text{slice, Epi, LB}} \quad (47a)$$

$$\text{s.t.} \quad (1), (3), (4), (8)-(10), (21b)-(21d), (25), (29b), (29c), (34c), (34d), (44b)-(44i), (44k), (44r)-(44v),$$

$$\tilde{x}_{b,u}^{v_l} \leq x_b^{v_l}, \quad \tilde{x}_{b,u}^{v_l} \leq \theta_{b,u}, \quad \tilde{x}_{b,u}^{v_l} \geq x_b^{v_l} + \theta_{b,u} - 1, \quad \tilde{x}_{b,u}^{v_l} \in \{0, 1\}, \quad (47b)$$

$$\tilde{y}_{b,u}^{v_h,v_l} \leq y_b^{v_h,v_l}, \quad \tilde{y}_{b,u}^{v_h,v_l} \leq \theta_{b,u}, \quad \tilde{y}_{b,u}^{v_h,v_l} \geq y_b^{v_h,v_l} + \theta_{b,u} - 1, \quad \tilde{y}_{b,u}^{v_h,v_l} \in \{0, 1\}, \quad (47c)$$

$$\tilde{z}_{b',b,u}^{v_l} \leq z_{b',b}^{v_l}, \quad \tilde{z}_{b',b,u}^{v_l} \leq \theta_{b,u}, \quad \tilde{z}_{b',b,u}^{v_l} \geq z_{b',b}^{v_l} + \theta_{b,u} - 1, \quad \tilde{z}_{b',b,u}^{v_l} \in \{0, 1\}, \quad (47d)$$

$$\tilde{t}_{b',b,u}^{v_h,v_l} \leq t_{b',b}^{v_h,v_l}, \quad \tilde{t}_{b',b,u}^{v_h,v_l} \leq \theta_{b,u}, \quad \tilde{t}_{b',b,u}^{v_h,v_l} \geq t_{b',b}^{v_h,v_l} + \theta_{b,u} - 1, \quad \tilde{t}_{b',b,u}^{v_h,v_l} \in \{0, 1\}, \quad (47e)$$

$$\tilde{w}_{b',b,u}^{v_h,v_l} \leq w_{b',b}^{v_h,v_l}, \quad \tilde{w}_{b',b,u}^{v_h,v_l} \leq \theta_{b,u}, \quad \tilde{w}_{b',b,u}^{v_h,v_l} \geq w_{b',b}^{v_h,v_l} + \theta_{b,u} - 1, \quad \tilde{w}_{b',b,u}^{v_h,v_l} \in \{0, 1\}, \quad (47f)$$

$$\tilde{o}_{b,u}^{v_l} \leq o_b^{v_l}, \quad \tilde{o}_{b,u}^{v_l} \leq \theta_{b,u}, \quad \tilde{o}_{b,u}^{v_l} \geq o_b^{v_l} + \theta_{b,u} - 1, \quad \tilde{o}_{b,u}^{v_l} \in \{0, 1\}, \quad (47g)$$

where $\check{\Upsilon} = [\check{\mathbf{x}}, \check{\mathbf{y}}, \check{\mathbf{z}}, \check{\mathbf{t}}, \check{\mathbf{w}}, \check{\mathbf{o}}]$, $\check{\mathbf{x}} = [\check{x}_{b,u}^{v_l}]$, $\check{\mathbf{y}} = [\check{y}_{b,u}^{v_h,v_l}]$, $\check{\mathbf{z}} = [\check{z}_{b',b,u}^{v_l}]$, $\check{\mathbf{t}} = [\check{t}_{b',b,u}^{v_h,v_l}]$, $\check{\mathbf{w}} = [\check{w}_{b',b,u}^{v_h,v_l}]$, $\check{\mathbf{o}} = [\check{o}_{b,u}^{v_l}]$ and $\bar{\$}_m^{\text{slice, Epi, LB}} = \sum_{u \in \mathcal{U}_m} \sum_{b \in \mathcal{B}} \bar{r}_{b,u}^{\text{Ac}} \psi_m - \sum_{u \in \mathcal{U}_m} \sum_{b \in \mathcal{B}} \sum_{n \in \mathcal{N}} (p_{b,u}^n \alpha_b^{\text{Pow}}) - \sum_{b \in \mathcal{B}} \sum_{n \in \mathcal{N}} (\nu_{b,m}^n W_s \alpha_b^{\text{Sub}}) -$

$$\begin{aligned} & \sum_{b \in \mathcal{B}} \sum_{u \in \mathcal{U}_m} \sum_{v_l \in \mathcal{V}} \Delta_{v_l} \left(\tilde{x}_{b,u}^{v_l} (s_{v_l} \mu_b^{\text{Cache}}) + \sum_{\substack{v_h \in \mathcal{V} \\ h > l}} \tilde{y}_{b,u}^{v_h,v_l} (s_{v_h} \mu_b^{\text{Cache}} + \phi_b^{v_h,v_l} \mu_b^{\text{Proc}}) + \right. \\ & \sum_{\substack{b' \in \mathcal{B} \\ b' \neq b}} \tilde{z}_{b',b,u}^{v_l} (s_{v_l} \mu_{b'}^{\text{Cache}} + r_{b',b}^{v_l} \alpha^{\text{FH}}) + \sum_{\substack{b' \in \mathcal{B} \\ b' \neq b}} \sum_{\substack{v_h \in \mathcal{V} \\ h > l}} \tilde{t}_{b',b,u}^{v_h,v_l} (s_{v_h} \mu_{b'}^{\text{Cache}} + \phi_{b'}^{v_h,v_l} \mu_{b'}^{\text{Proc}} + r_{b',b}^{v_l} \alpha^{\text{FH}}) + \\ & \left. \sum_{\substack{b' \in \mathcal{B} \\ b' \neq b}} \sum_{\substack{v_h \in \mathcal{V} \\ h > l}} \tilde{w}_{b',b,u}^{v_h,v_l} (s_{v_h} \mu_{b'}^{\text{Cache}} + r_{b',b}^{v_h} \alpha^{\text{FH}} + \phi_b^{v_h,v_l} \mu_b^{\text{Proc}}) + \tilde{o}_{b,u}^{v_l} (r_{0,b}^{v_l} \alpha^{\text{BH}}) \right). \end{aligned}$$

APPENDIX E

PROOF OF PROPOSITION 2

Each iteration κ_1 in the proposed Algorithm 1 for solving (29) consists of two main steps. In the first step, we find $(\mathbf{p}_{\kappa_1}, \phi_{\kappa_1}, \mathbf{r}_{\kappa_1}^{\text{FH}}, \mathbf{r}_{\kappa_1}^{\text{BH}})$ by solving (29) for a fixed $(\Upsilon_{\kappa_1-1}, \boldsymbol{\rho}_{\kappa_1-1}, \boldsymbol{\tau}_{\kappa_1-1}, \boldsymbol{\theta}_{\kappa_1-1})$ using an equivalent transformation method and subsequently applying the iterative SCA Algorithm 2 which provides a local optimum solution for (29) that is proved in **Proposition 3**. In this line, we have the following relation

$$\bar{\$}_{\text{tot}}(\mathbf{p}_{\kappa_1-1}, \phi_{\kappa_1-1}, \mathbf{r}_{\kappa_1-1}^{\text{FH}}, \mathbf{r}_{\kappa_1-1}^{\text{BH}}, \Upsilon_{\kappa_1-1}, \boldsymbol{\rho}_{\kappa_1-1}, \boldsymbol{\tau}_{\kappa_1-1}, \boldsymbol{\theta}_{\kappa_1-1}) \leq \bar{\$}_{\text{tot}}(\mathbf{p}_{\kappa_1}, \phi_{\kappa_1}, \mathbf{r}_{\kappa_1}^{\text{FH}}, \mathbf{r}_{\kappa_1}^{\text{BH}}, \Upsilon_{\kappa_1-1}, \boldsymbol{\rho}_{\kappa_1-1}, \boldsymbol{\tau}_{\kappa_1-1}, \boldsymbol{\theta}_{\kappa_1-1}). \quad (48)$$

In the second step of iteration κ_1 , we find $(\Upsilon_{\kappa_1}, \boldsymbol{\rho}_{\kappa_1}, \boldsymbol{\tau}_{\kappa_1}, \boldsymbol{\theta}_{\kappa_1})$ by solving (29) for the given $(\mathbf{p}_{\kappa_1}, \phi_{\kappa_1}, \mathbf{r}_{\kappa_1}^{\text{FH}}, \mathbf{r}_{\kappa_1}^{\text{BH}})$ from the previous step. In doing so, the INLP problem (29) is transformed into a IDCP from in (44) which is efficiently solved by using CVX with the internal solver MOSEK. Using the fact that CVX with the MOSEK solver improves the objective function (44a) or the objective function of its equivalent problem (29) for the given $(\mathbf{p}_{\kappa_1}, \phi_{\kappa_1}, \mathbf{r}_{\kappa_1}^{\text{FH}}, \mathbf{r}_{\kappa_1}^{\text{BH}})$, the following relation holds

$$\bar{\$}_{\text{tot}}(\mathbf{p}_{\kappa_1}, \phi_{\kappa_1}, \mathbf{r}_{\kappa_1}^{\text{FH}}, \mathbf{r}_{\kappa_1}^{\text{BH}}, \Upsilon_{\kappa_1-1}, \boldsymbol{\rho}_{\kappa_1-1}, \boldsymbol{\tau}_{\kappa_1-1}, \boldsymbol{\theta}_{\kappa_1-1}) \leq \bar{\$}_{\text{tot}}(\mathbf{p}_{\kappa_1}, \phi_{\kappa_1}, \mathbf{r}_{\kappa_1}^{\text{FH}}, \mathbf{r}_{\kappa_1}^{\text{BH}}, \Upsilon_{\kappa_1}, \boldsymbol{\rho}_{\kappa_1}, \boldsymbol{\tau}_{\kappa_1}, \boldsymbol{\theta}_{\kappa_1}). \quad (49)$$

According to (48) and (49), it can be easily observed that after each iteration κ_1 of Algorithm 1, the objective function (29a) is either improved or remains constant. Essentially, when the iterations in Algorithm 1 continue, it will converge to a locally optimal solution. Note that since the solution approach in the first step of Algorithm 1, i.e, finding $(\mathbf{p}_{\kappa_1}, \phi_{\kappa_1}, \mathbf{r}_{\kappa_1}^{\text{FH}}, \mathbf{r}_{\kappa_1}^{\text{BH}})$ basically follows the SCA approach which converges to a locally optimal solution, the globally optimal solution $(\mathbf{p}_{\kappa_1}, \phi_{\kappa_1}, \mathbf{r}_{\kappa_1}^{\text{FH}}, \mathbf{r}_{\kappa_1}^{\text{BH}})$ can not be guaranteed and the performance gap from this locally optimal solution and the global solution is also unknown. To this end, their corresponding solutions $(\Upsilon_{\kappa_1}, \boldsymbol{\rho}_{\kappa_1}, \boldsymbol{\tau}_{\kappa_1}, \boldsymbol{\theta}_{\kappa_1})$ maybe different. Accordingly, alternative Algorithm 1 cannot guarantee the global optimality of the solution for (29) and what can be proved is only the local optimality of the solution. Nevertheless, in [33], [42] is noted that the SCA method often empirically converges to a globally optimal solution.

APPENDIX F

PROOF OF PROPOSITION 3

In order to prove **Proposition 3**, we first prove that the proposed SCA-based Algorithm 2 generates a sequence of improved feasible solutions in equivalent problem of (31) which is formulated in (34). As discussed, in each iteration κ_2 of the SCA approach, $g_{b,u}^n(\mathbf{p}_{\kappa_2})$ is approximated with its first order Taylor series in (11) and $f_{b,u}^n(\mathbf{p}_{\kappa_2})$ is approximated with its first order Taylor series in (34e)-(34i). Indeed, $\nabla g_{b,u}^n(\mathbf{p}_{\kappa_2-1})$ and $\nabla f_{b,u}^n(\mathbf{p}_{\kappa_2-1})$ are supergradient functions of $g_{b,u}^n(\mathbf{p}_{\kappa_2-1})$ and $f_{b,u}^n(\mathbf{p}_{\kappa_2-1})$ for iteration $\kappa_2 - 1$, respectively. Since $g_{b,u}^n(\mathbf{p}_{\kappa_2})$ and $f_{b,u}^n(\mathbf{p}_{\kappa_2})$ are concave, it must be hold

$$g_{b,u}^n(\mathbf{p}_{\kappa_2}) \leq g_{b,u}^n(\mathbf{p}_{\kappa_2-1}) + \nabla g_{b,u}^n(\mathbf{p}_{\kappa_2-1})(\mathbf{p}_{\kappa_2} - \mathbf{p}_{\kappa_2-1}), \quad (50)$$

$$f_{b,u}^n(\mathbf{p}_{\kappa_2}) \leq f_{b,u}^n(\mathbf{p}_{\kappa_2-1}) + \nabla f_{b,u}^n(\mathbf{p}_{\kappa_2-1})(\mathbf{p}_{\kappa_2} - \mathbf{p}_{\kappa_2-1}), \quad (51)$$

at each iteration κ_2 , respectively. Using (40) and (43), the ergodic access data rate function $\bar{r}_{b,u}^n(\mathbf{p}_{\kappa_2})$ in (35) is approximated to a concave form $\hat{r}_{b,u}^n(\mathbf{p}_{\kappa_2})$ in (11) and also to a convex form $\tilde{r}_{b,u}^n(\mathbf{p}_{\kappa_2})$ in (34e)-(34i) at each iteration κ_2 . According to (35) and (50) it can be easily shown that the following relations hold

$$\begin{aligned} \bar{r}_{b,u}^n(\mathbf{p}_{\kappa_2}) &= \mathbb{E}_{\mathbf{h}} \{ f_{b,u}^n(\mathbf{p}_{\kappa_2}) - g_{b,u}^n(\mathbf{p}_{\kappa_2}) \} \geq \\ \hat{r}_{b,u}^n(\mathbf{p}_{\kappa_2}) &= \mathbb{E}_{\mathbf{h}} \{ f_{b,u}^n(\mathbf{p}_{\kappa_2}) - g_{b,u}^n(\mathbf{p}_{\kappa_2-1}) - \nabla g_{b,u}^n(\mathbf{p}_{\kappa_2-1})(\mathbf{p}_{\kappa_2} - \mathbf{p}_{\kappa_2-1}) \}. \end{aligned} \quad (52)$$

Moreover, based on (35) and (51), we have

$$\begin{aligned} \bar{r}_{b,u}^n(\mathbf{p}_{\kappa_2}) &= \mathbb{E}_{\mathbf{h}} \{ f_{b,u}^n(\mathbf{p}_{\kappa_2}) - g_{b,u}^n(\mathbf{p}_{\kappa_2}) \} \leq \\ \tilde{r}_{b,u}^n(\mathbf{p}_{\kappa_2}) &= \mathbb{E}_{\mathbf{h}} \{ f_{b,u}^n(\mathbf{p}_{\kappa_2-1}) + \nabla f_{b,u}^n(\mathbf{p}_{\kappa_2-1})(\mathbf{p}_{\kappa_2} - \mathbf{p}_{\kappa_2-1}) - g_{b,u}^n(\mathbf{p}_{\kappa_2}) \}. \end{aligned} \quad (53)$$

Besides, after solving the convex approximated problem of (34) in each iteration κ_2 , the following inequalities hold

$$\sum_{b \in \mathcal{B}} \sum_{n=1}^N \hat{r}_{b,u}^n(\mathbf{p}_{\kappa_2}) \geq R_m^{\min}, \forall m \in \mathcal{M}, u \in \mathcal{U}_m, \quad (54)$$

$$y_b^{v_h, v_l} \frac{\sum_{n=1}^N \tilde{r}_{b,u}^n(\mathbf{p}_{\kappa_2})}{s_{v_l}} \leq \frac{\phi_b^{v_h, v_l}}{\eta^{v_h, v_l} N_{\text{Cycle}}^{v_h, v_l}} y_b^{v_h, v_l}, \quad (55)$$

$$z_{b',b}^{v_l} \sum_{n=1}^N \tilde{r}_{b,u}^n(\mathbf{p}_{\kappa_2}) \leq r_{b',b}^{v_l} z_{b',b}^{v_l}, \quad (56)$$

$$t_{b',b}^{v_h,v_l} \sum_{n=1}^N \tilde{r}_{b,u}^n(\mathbf{p}_{\kappa_2}) \leq t_{b',b}^{v_h,v_l} r_{b',b}^{v_l}, \quad (57)$$

$$w_{b',b}^{v_h,v_l} \frac{\sum_{n=1}^N \tilde{r}_{b,u}^n(\mathbf{p}_{\kappa_2})}{s_{v_l}} \leq w_{b',b}^{v_h,v_l} \frac{\phi_b^{v_h,v_l}}{\eta^{v_h,v_l} N_{\text{Cycle}}^{v_h,v_l}}, \quad (58)$$

and

$$o_b^{v_l} \sum_{n=1}^N \tilde{r}_{b,u}^n(\mathbf{p}_{\kappa_2}) \leq o_b^{v_l} r_{0,b}^{v_l}. \quad (59)$$

From (52)-(59), it can be concluded that

$$\sum_{b \in \mathcal{B}} \tilde{r}_{b,u}^n(\mathbf{p}_{\kappa_2}) \geq R_m^{\min}, \forall m \in \mathcal{M}, u \in \mathcal{U}_m, \quad (60)$$

$$y_b^{v_h,v_l} \frac{\tilde{r}_{b,u}^n(\mathbf{p}_{\kappa_2})}{s_{v_l}} \leq \frac{\phi_b^{v_h,v_l}}{\eta^{v_h,v_l} N_{\text{Cycle}}^{v_h,v_l}} y_b^{v_h,v_l}, \quad (61)$$

$$z_{b',b}^{v_l} \tilde{r}_{b,u}^n(\mathbf{p}_{\kappa_2}) \leq r_{b',b}^{v_l} z_{b',b}^{v_l}, \quad (62)$$

$$t_{b',b}^{v_h,v_l} \tilde{r}_{b,u}^n(\mathbf{p}_{\kappa_2}) \leq t_{b',b}^{v_h,v_l} r_{b',b}^{v_l}, \quad (63)$$

$$w_{b',b}^{v_h,v_l} \frac{\tilde{r}_{b,u}^n(\mathbf{p}_{\kappa_2})}{s_{v_l}} \leq w_{b',b}^{v_h,v_l} \frac{\phi_b^{v_h,v_l}}{\eta^{v_h,v_l} N_{\text{Cycle}}^{v_h,v_l}}, \quad (64)$$

and

$$o_b^{v_l} \tilde{r}_{b,u}^n(\mathbf{p}_{\kappa_2}) \leq o_b^{v_l} r_{0,b}^{v_l}, \quad (65)$$

which means the optimal solution generated for the convex approximated problem of (34) at each iteration κ_2 is feasible with respect to the nonconvex problem (34). Moreover, based on (52), we have

$$\begin{aligned} & \sum_{m \in \mathcal{M}} \left(\sum_{u \in \mathcal{U}_m} \sum_{b \in \mathcal{B}} \tilde{r}_{b,u}^{\text{Ac}}(\mathbf{p}_{\kappa_2}^*) \psi_m - \sum_{u \in \mathcal{U}_m} \sum_{b \in \mathcal{B}} \sum_{n \in \mathcal{N}} \left(p_{b,u}^{n,(\kappa_2)} \alpha_b^{\text{Pow}} \right) - \sum_{b \in \mathcal{B}} \sum_{n \in \mathcal{N}} \left(\max_{u \in \mathcal{U}_m} \{\tau_{b,u}^n\} W_s \alpha_b^{\text{Sub}} \right) \right) \\ & - \sum_{b \in \mathcal{B}} \min \left\{ \sum_{u \in \mathcal{U}_m} \theta_{b,u}, 1 \right\} \bar{\Phi}_b^{\text{Cost,RRS}} \geq \sum_{m \in \mathcal{M}} \left(\sum_{u \in \mathcal{U}_m} \sum_{b \in \mathcal{B}} \sum_{n \in \mathcal{N}} \left(\hat{r}_{b,u}^n(\mathbf{p}_{\kappa_2}^*) \right) \psi_m - \sum_{u \in \mathcal{U}_m} \sum_{b \in \mathcal{B}} \sum_{n \in \mathcal{N}} \left(p_{b,u}^n \alpha_b^{\text{Pow}} \right) \right. \\ & \quad \left. - \sum_{b \in \mathcal{B}} \sum_{n \in \mathcal{N}} \left(\max_{u \in \mathcal{U}_m} \{\tau_{b,u}^n\} W_s \alpha_b^{\text{Sub}} \right) - \sum_{b \in \mathcal{B}} \min \left\{ \sum_{u \in \mathcal{U}_m} \theta_{b,u}, 1 \right\} \bar{\Phi}_b^{\text{Cost,RRS}} \right). \quad (66) \end{aligned}$$

By using the fact that the DCP approximated problem of (34) can be efficiently solved at each iteration κ_2 , where the globally optimal solution is in the feasible region of (34), it can be derived that

$$\begin{aligned}
& \sum_{m \in \mathcal{M}} \left(\sum_{u \in \mathcal{U}_m} \sum_{b \in \mathcal{B}} \sum_{n \in \mathcal{N}} (\hat{r}_{b,u}^n(\mathbf{p}_{\kappa_2}^*)) \psi_m - \sum_{u \in \mathcal{U}_m} \sum_{b \in \mathcal{B}} \sum_{n \in \mathcal{N}} (p_{b,u}^{n,(\kappa_2)*} \alpha_b^{\text{Pow}}) - \sum_{b \in \mathcal{B}} \sum_{n \in \mathcal{N}} \left(\max_{u \in \mathcal{U}_m} \{\tau_{b,u}^n\} W_s \alpha_b^{\text{Sub}} \right) \right. \\
& \quad \left. - \sum_{b \in \mathcal{B}} \min \left\{ \sum_{u \in \mathcal{U}_m} \theta_{b,u}, 1 \right\} \bar{\mathbb{S}}_b^{\text{Cost,RRS}} \right) = \max_{\phi_{\kappa_2}, \mathbf{p}_{\kappa_2}, \mathbf{r}_{\kappa_2}^{\text{BH}}, \mathbf{r}_{\kappa_2}^{\text{FH}}} \sum_{m \in \mathcal{M}} \left(\sum_{u \in \mathcal{U}_m} \sum_{b \in \mathcal{B}} \sum_{n \in \mathcal{N}} (\hat{r}_{b,u}^n(\mathbf{p}_{\kappa_2})) \psi_m - \right. \\
& \quad \sum_{u \in \mathcal{U}_m} \sum_{b \in \mathcal{B}} \sum_{n \in \mathcal{N}} (p_{b,u}^{n,(\kappa_2)} \alpha_b^{\text{Pow}}) - \sum_{b \in \mathcal{B}} \sum_{n \in \mathcal{N}} \left(\max_{u \in \mathcal{U}_m} \{\tau_{b,u}^n\} W_s \alpha_b^{\text{Sub}} \right) - \sum_{b \in \mathcal{B}} \min \left\{ \sum_{u \in \mathcal{U}_m} \theta_{b,u}, 1 \right\} \bar{\mathbb{S}}_b^{\text{Cost,RRS}} \Big) \geq \\
& \quad \sum_{m \in \mathcal{M}} \left(\sum_{u \in \mathcal{U}_m} \sum_{b \in \mathcal{B}} \sum_{n \in \mathcal{N}} (\mathbb{E}_{\mathbf{h}} \{f_{b,u}^n(\mathbf{p}_{\kappa_2-1}) - g_{b,u}^n(\mathbf{p}_{\kappa_2-1}) - \nabla g_{b,u}^n(\mathbf{p}_{\kappa_2-1})(\mathbf{p}_{\kappa_2-1} - \mathbf{p}_{\kappa_2-1})\}) \psi_m - \right. \\
& \quad \sum_{u \in \mathcal{U}_m} \sum_{b \in \mathcal{B}} \sum_{n \in \mathcal{N}} (p_{b,u}^{n,(\kappa_2-1)} \alpha_b^{\text{Pow}}) - \sum_{b \in \mathcal{B}} \sum_{n \in \mathcal{N}} \left(\max_{u \in \mathcal{U}_m} \{\tau_{b,u}^n\} W_s \alpha_b^{\text{Sub}} \right) - \sum_{b \in \mathcal{B}} \min \left\{ \sum_{u \in \mathcal{U}_m} \theta_{b,u}, 1 \right\} \bar{\mathbb{S}}_b^{\text{Cost,RRS}} \Big) = \\
& \quad \sum_{m \in \mathcal{M}} \left(\sum_{u \in \mathcal{U}_m} \sum_{b \in \mathcal{B}} \sum_{n \in \mathcal{N}} (\mathbb{E}_{\mathbf{h}} \{f_{b,u}^n(\mathbf{p}_{\kappa_2-1}) - g_{b,u}^n(\mathbf{p}_{\kappa_2-1})\}) \psi_m - \sum_{u \in \mathcal{U}_m} \sum_{b \in \mathcal{B}} \sum_{n \in \mathcal{N}} (p_{b,u}^{n,(\kappa_2-1)} \alpha_b^{\text{Pow}}) - \right. \\
& \quad \sum_{b \in \mathcal{B}} \sum_{n \in \mathcal{N}} \left(\max_{u \in \mathcal{U}_m} \{\tau_{b,u}^n\} W_s \alpha_b^{\text{Sub}} \right) - \sum_{b \in \mathcal{B}} \min \left\{ \sum_{u \in \mathcal{U}_m} \theta_{b,u}, 1 \right\} \bar{\mathbb{S}}_b^{\text{Cost,RRS}} \Big) = \\
& \quad \sum_{m \in \mathcal{M}} \left(\sum_{u \in \mathcal{U}_m} \sum_{b \in \mathcal{B}} \sum_{n \in \mathcal{N}} (\bar{r}_{b,u}^n(\mathbf{p}_{\kappa_2-1})) \psi_m - \sum_{u \in \mathcal{U}_m} \sum_{b \in \mathcal{B}} \sum_{n \in \mathcal{N}} (p_{b,u}^{n,(\kappa_2-1)} \alpha_b^{\text{Pow}}) - \sum_{b \in \mathcal{B}} \sum_{n \in \mathcal{N}} \left(\max_{u \in \mathcal{U}_m} \{\tau_{b,u}^n\} W_s \alpha_b^{\text{Sub}} \right) \right. \\
& \quad \left. - \sum_{b \in \mathcal{B}} \min \left\{ \sum_{u \in \mathcal{U}_m} \theta_{b,u}, 1 \right\} \bar{\mathbb{S}}_b^{\text{Cost,RRS}} \right). \quad (67)
\end{aligned}$$

According to (66) and (67), it is obvious that

$$\begin{aligned}
& \sum_{m \in \mathcal{M}} \left(\sum_{u \in \mathcal{U}_m} \sum_{b \in \mathcal{B}} \bar{r}_{b,u}^{\text{Ac}}(\mathbf{p}_{\kappa_2}^*) \psi_m - \sum_{u \in \mathcal{U}_m} \sum_{b \in \mathcal{B}} \sum_{n \in \mathcal{N}} (p_{b,u}^{n,(\kappa_2)} \alpha_b^{\text{Pow}}) - \sum_{b \in \mathcal{B}} \sum_{n \in \mathcal{N}} \left(\max_{u \in \mathcal{U}_m} \{\tau_{b,u}^n\} W_s \alpha_b^{\text{Sub}} \right) \right. \\
& \quad \left. - \sum_{b \in \mathcal{B}} \min \left\{ \sum_{u \in \mathcal{U}_m} \theta_{b,u}, 1 \right\} \bar{\mathbb{S}}_b^{\text{Cost,RRS}} \right) \geq \sum_{m \in \mathcal{M}} \left(\sum_{u \in \mathcal{U}_m} \sum_{b \in \mathcal{B}} \sum_{n \in \mathcal{N}} (\bar{r}_{b,u}^n(\mathbf{p}_{\kappa_2-1})) \psi_m - \right. \\
& \quad \sum_{u \in \mathcal{U}_m} \sum_{b \in \mathcal{B}} \sum_{n \in \mathcal{N}} (p_{b,u}^{n,(\kappa_2-1)} \alpha_b^{\text{Pow}}) - \sum_{b \in \mathcal{B}} \sum_{n \in \mathcal{N}} \left(\max_{u \in \mathcal{U}_m} \{\tau_{b,u}^n\} W_s \alpha_b^{\text{Sub}} \right) - \sum_{b \in \mathcal{B}} \min \left\{ \sum_{u \in \mathcal{U}_m} \theta_{b,u}, 1 \right\} \bar{\mathbb{S}}_b^{\text{Cost,RRS}} \Big), \quad (68)
\end{aligned}$$

which means after each iteration κ_2 of the proposed SCA approach for solving (34), the objective function (34a) which is exactly the same as (31a) is improved (increased) or remains constant. Accordingly, the proposed algorithm for solving (31) will converge to a local optimum solution.

REFERENCES

- [1] W. Jiang, G. Feng, and S. Qin, "Optimal cooperative content caching and delivery policy for heterogeneous cellular networks," *IEEE Transactions on Mobile Computing*, vol. 16, no. 5, pp. 1382–1393, May 2017.
- [2] N. Golrezaei, K. Shanmugam, A. G. Dimakis, A. F. Molisch, and G. Caire, "Femtocaching: Wireless video content delivery through distributed caching helpers," in *Proc. IEEE INFOCOM*, Orlando, FL, USA, Mar. 2012, pp. 1107–1115.
- [3] Cisco Visual Networking Index, "Global mobile data traffic forecast update, 2016–2021," *White Paper c11-520862*, March 28, 2017.
- [4] H. A. Pedersen and S. Dey, "Enhancing mobile video capacity and quality using rate adaptation, RAN caching and processing," *IEEE/ACM Transactions on Networking*, vol. 24, no. 2, pp. 996–1010, Apr. 2016.
- [5] T. X. Tran, P. Pandey, A. Hajisami, and D. Pompili, "Collaborative multi-bitrate video caching and processing in mobile-edge computing networks," in *Proc. 13th Annual Conference on Wireless On-demand Network Systems and Services (WONS)*, Jackson, WY, USA, Feb. 2017, pp. 165–172.
- [6] T. X. Tran, A. Hajisami, P. Pandey, and D. Pompili, "Collaborative mobile edge computing in 5G networks: New paradigms, scenarios, and challenges," *IEEE Communications Magazine*, vol. 55, no. 4, pp. 54–61, Apr. 2017.
- [7] H. Ahleghagh and S. Dey, "Video-aware scheduling and caching in the radio access network," *IEEE/ACM Transactions on Networking*, vol. 22, no. 5, pp. 1444–1462, Oct. 2014.
- [8] X. Xu, J. Liu, and X. Tao, "Mobile edge computing enhanced adaptive bitrate video delivery with joint cache and radio resource allocation," *IEEE Access*, vol. 5, pp. 16 406–16 415, Aug. 2017.
- [9] L. Wei, J. Cai, C. H. Foh, and B. He, "QoS-aware resource allocation for video transcoding in clouds," *IEEE Transactions on Circuits and Systems for Video Technology*, vol. 27, no. 1, pp. 49–61, Jan. 2017.
- [10] Y. Mao, J. Zhang, and K. B. Letaief, "Dynamic computation offloading for mobile-edge computing with energy harvesting devices," *IEEE Journal on Selected Areas in Communications*, vol. 34, no. 12, pp. 3590–3605, Dec. 2016.
- [11] C. You, K. Huang, H. Chae, and B. H. Kim, "Energy-efficient resource allocation for mobile-edge computation offloading," *IEEE Transactions on Wireless Communications*, vol. 16, no. 3, pp. 1397–1411, Mar. 2017.
- [12] J. Ren, G. Yu, Y. Cai, and Y. He, "Latency optimization for resource allocation in mobile-edge computation offloading," *arXiv preprint arXiv:1704.00163v1*, Apr. 2017.
- [13] K. Wang, H. Li, F. R. Yu, and W. Wei, "Virtual resource allocation in software-defined information-centric cellular networks with device-to-device communications and imperfect CSI," *IEEE Transactions on Vehicular Technology*, vol. 65, no. 12, pp. 10 011–10 021, Dec. 2016.
- [14] K. Wang, F. R. Yu, and H. Li, "Information-centric virtualized cellular networks with device-to-device (D2D) communications," *IEEE Transactions on Vehicular Technology*, vol. 65, no. 11, pp. 9319–9329, Nov. 2016.
- [15] X. Zhang and Q. Zhu, "Information-centric network virtualization for QoS provisioning over software defined wireless networks," in *Proc. IEEE Military Communications Conference (MILCOM)*, Baltimore, Maryland, Nov. 2016, pp. 1028–1033.
- [16] Z. Chen, J. Lee, T. Q. S. Quek, and M. Kountouris, "Cooperative caching and transmission design in cluster-centric small cell networks," *IEEE Transactions on Wireless Communications*, vol. 16, no. 5, pp. 3401–3415, May 2017.
- [17] J. Liu, B. Bai, J. Zhang, and K. B. Letaief, "Cache placement in fog-RANs: From centralized to distributed algorithms," *IEEE Transactions on Wireless Communications*, vol. 16, no. 11, pp. 7039–7051, Nov. 2017.
- [18] R. G. Stephen and R. Zhang, "Green OFDMA resource allocation in cache-enabled CRAN," in *Proc. IEEE Online Conference on Green Communications (OnlineGreenComm)*, Piscataway, NJ, USA, Nov. 2016, pp. 70–75.

- [19] Z. Tan, X. Li, F. R. Yu, L. Chen, H. Ji, and V. C. M. Leung, "Joint access selection and resource allocation in cache-enabled HCNs with D2D communications," in *Proc. IEEE Wireless Communications and Networking Conference (WCNC)*, San Francisco, CA, USA, Mar. 2017, pp. 1–6.
- [20] X. Peng, J. C. Shen, J. Zhang, and K. B. Letaief, "Backhaul-aware caching placement for wireless networks," in *Proc. IEEE Global Communications Conference (GLOBECOM)*, San Diego, CA, USA, Dec. 2015, pp. 1–6.
- [21] W. C. Ao and K. Psounis, "Fast content delivery via distributed caching and small cell cooperation," *IEEE Transactions on Mobile Computing*, vol. PP, no. 99, pp. 1–1, 2017.
- [22] X. Li, X. Wang, S. Xiao, and V. C. M. Leung, "Delay performance analysis of cooperative cell caching in future mobile networks," in *Proc. IEEE International Conference on Communications (ICC)*, London, England, June 2015, pp. 5652–5657.
- [23] Z. Ding, P. Fan, G. K. Karagiannidis, R. Schober, and H. V. Poor, "NOMA assisted wireless caching: Strategies and performance analysis," *arXiv preprint arXiv:1709.06951v2*, Jan. 2018.
- [24] C. Liang, F. R. Yu, H. Yao, and Z. Han, "Virtual resource allocation in information-centric wireless networks with virtualization," *IEEE Transactions on Vehicular Technology*, vol. 65, no. 12, pp. 9902–9914, Dec. 2016.
- [25] G. Gao, H. Hu, Y. Wen, and C. Westphal, "Resource provisioning and profit maximization for transcoding in clouds: A two-timescale approach," *IEEE Transactions on Multimedia*, vol. 19, no. 4, pp. 836–848, Apr. 2017.
- [26] C. F. Kao and C. N. Lee, "Aggregate profit-based caching replacement algorithms for streaming media transcoding proxy systems," *IEEE Transactions on Multimedia*, vol. 9, no. 2, pp. 221–230, Feb. 2007.
- [27] F. Cheng, Y. Yu, Z. Zhao, N. Zhao, Y. Chen, and H. Lin, "Power allocation for cache-aided small-cell networks with limited backhaul," *IEEE Access*, vol. 5, pp. 1272–1283, Jan. 2017.
- [28] Y. Sun, D. W. K. Ng, Z. Ding, and R. Schober, "Optimal joint power and subcarrier allocation for MC-NOMA systems," in *Proc. IEEE Global Communications Conference (GLOBECOM)*, Washington, DC, USA, Dec. 2016.
- [29] Y. Fu, L. Salan, C. W. Sung, C. S. Chen, and M. Coupechoux, "Double iterative waterfilling for sum rate maximization in multicarrier NOMA systems," in *Proc. IEEE International Conference on Communications (ICC)*, Paris, France, May 2017.
- [30] Y. Sun, D. W. K. Ng, Z. Ding, and R. Schober, "Optimal joint power and subcarrier allocation for full-duplex multicarrier non-orthogonal multiple access systems," *IEEE Transactions on Communications*, vol. 65, no. 3, pp. 1077–1091, Mar. 2017.
- [31] S. H. Park, O. Simeone, and S. S. Shitz, "Joint optimization of cloud and edge processing for fog radio access networks," *IEEE Transactions on Wireless Communications*, vol. 15, no. 11, pp. 7621–7632, Nov. 2016.
- [32] L. Lei, D. Yuan, C. K. Ho, and S. Sun, "Joint optimization of power and channel allocation with non-orthogonal multiple access for 5G cellular systems," in *Proc. IEEE Global Communications Conference (GLOBECOM)*, San Diego, CA, USA, Dec. 2015.
- [33] D. T. Ngo, S. Khakurel, and T. Le-Ngoc, "Joint subchannel assignment and power allocation for OFDMA femtocell networks," *IEEE Transactions on Wireless Communications*, vol. 13, no. 1, pp. 342–355, Jan. 2014.
- [34] N. Mokari, F. Alavi, S. Parsaeefard, and T. Le-Ngoc, "Limited-feedback resource allocation in heterogeneous cellular networks," *IEEE Transactions on Vehicular Technology*, vol. 65, no. 4, pp. 2509–2521, Apr. 2016.
- [35] M. Grant and S. Boyd, "CVX: Matlab software for disciplined convex programming, version 2.1," Mar. 2014 [Online] Available: <http://cvxr.com/cvx>.
- [36] <https://www.mosek.com/products/mosek>.
- [37] GreenTouch, *Mobile communications WG architecture doc2: Reference scenarios*, May 2013.

- [38] A. P. Miettinen and J. K. Nurminen, “Energy efficiency of mobile clients in cloud computing,” in *Proc. USENIX Conference on Hot Topics in Cloud Computing (HotCloud)*, Boston, MA, Jun. 2010.
- [39] A. Ben-Tal and A. Nemirovski, *Lectures on modern convex optimization analysis, algorithms, and engineering applications*. vol. 2. Siam, 2001.
- [40] M. Tao, E. Chen, H. Zhou, and W. Yu, “Content-centric sparse multicast beamforming for cache-enabled cloud RAN,” *IEEE Transactions on Wireless Communications*, vol. 15, no. 9, pp. 6118–6131, Sep. 2016.
- [41] S. Boyd and L. Vandenberghe, *Convex Optimization*. Cambridge University Press, 2009.
- [42] H. H. Kha, H. D. Tuan, and H. H. Nguyen, “Fast global optimal power allocation in wireless networks by local D.C. programming,” *IEEE Transactions on Wireless Communications*, vol. 11, no. 2, pp. 510–515, Feb. 2012.